In search of the first animals

Shirin Baydjanova

Masters of Research

03/11/2015

Macquarie University, Department of Earth and Planetary Sciences

Macquarie Organic Geochemistry Laboratory

ARC Centre of Excellence for Core to Crust Fluid Systems (CCFS)

Contents

Shirin Baydjanova

Shirin Baydjanova

Table of figures

Shirin Baydjanova

Shirin Baydjanova

Shirin Baydjanova

Abstract

The earliest proven fossils of multicellular animals are accepted to be those of the Ediacaran biota (*ca* 580 - 541 Ma), although some pre-Ediacaran samples from the Rasthof Formation of the Congo craton, Namibia, and from the Balcanoona Formation in the Northern Flinders Ranges, South Australia, have been claimed to contain fossils of the proto-sponges. The current study assesses samples from the above localities for the thermal maturity of the organic matter and the presence of sponge biomarkers.

A combination of SEM, Raman and FTIR spectroscopy, and GC-MS techniques shows that the organic matter in the studied samples is over-mature for oil generation, with an equivalent vitrinite reflectance (R_0) $\geq$ 1.4%. The Namibian samples (three dolostones from the Rasthof and Berg Aukas Formations) are more mature than the Australian samples (two siltstones from the Tapley Hill Formation and a dolomitic limestone from the Balcanoona Formation). The former are of chlorite zone metamorphic grade, while the latter exhibit characteristics of both pre-greenschist and greenschist (chlorite zone) metamorphism.

No samples yielded sterane biomarkers specific to sponges, or any other biomarkers, including the normally ubiquitous hopanes. The absence of intact biomarkers can be attributed to their thermal destruction during late catagenesis and early metamorphism.

Keywords: Cryogenian, sponge fossils, biomarkers, South Australia, Northern Namibia.

Statement of originality

No part of this thesis has previously been submitted for a degree at this or any other university. The work described in this thesis is entirely that of the author, except where reference is made to previously published or unpublished work.

Shirin Baydjanova

Acknowledgements

Shirin Baydjanova

Chapter 1. Introduction

1.1   Background

1.1.1 Earliest animals

Today, Earth is populated by many forms of life. Animals - vertebrates and invertebrates - can be found in any climatic zone, with *Homo sapiens* being the dominant group. But how and when animals appeared on Earth is the question we are still trying to answer.

The Ediacaran biota (*ca* 580 - 541 Ma) is considered to be the first proven fossil findings of the animals (Grazhdankin, 2004, McCall, 2006, Narbonne, 2008, Laflamme, 2010, Narbonne et al., 2012). There are some claims of the pre-Ediacaran animal fossil findings (Love et al., 2009, Maloof et al., 2010, Wallace et al., 2014). This study aims to test some of these claims using spectroscopic and organic geochemistry techniques.

1.1.2 Early life and the Snowball Earth

About 2.4 – 2.3 Ga the Earth's atmosphere changed from largely anoxic to a moderately oxygenated (Farquhar and Wing, 2003, Canfield, 2005, Holland, 2006). This shift is called the Great Oxygenation Event (GOE). During the GOE, the oxygen increased to ~ 1-2 % of modern oxygen level. These changes are thought to be the reason for the emergence of photosynthetic life on Earth. Till ~ 850 Ma ago, the oxygen level did not significantly changed, however, between 850 Ma and 540 Ma the amount of oxygen had risen to ~ 20% of modern level (Holland, 2006). The fluctuations in oxygen level resulted, probably, in the development of more complex life forms such as multicellularity, the appearance of eukaryotes, and eukaryotes divergence (Knoll, 2003, Johnston et al., 2009).

The Snowball Earth conditions refer to the time of two great glaciations – the Sturtian (~720 Ma) and the Marinoan (~635 Ma) (Fromhold and Wallace, 2011). There are ongoing debates about the climatic conditions the Earth experienced at those times; whether its surface was completely covered by ice (the Hardball Earth) or if there were large areas of open waters in the tropics (the Slushball Earth) (Pierrehumbert et al., 2011). Recent fossil discoveries of

Shirin Baydjanova

unicellular and multicellular organisms (both prokaryotes and eukaryotes) suggest that slushball conditions were more likely, otherwise the survival of complex life could not have been possible (Corsetti et al., 2003, Moczydłowska, 2008).

1.1.3 The Snowball Earth survivors

The fossil records show that multicellular algae evolved before the Snowball Earth events but diversified after the Marinoan glaciation, and at least some lineages of different algal clades survived through the Cryogenian. Cyanobacteria and stromatolites also survived all Neoproterozoic glaciations. Acritarchs (usually interpreted as resting cysts of photoautotrophic eukaryotes) also survived despite significant diversity loss between the Sturtian and the Marinoan (Figure 1.1.1) (Xiao, 2004, Moczydłowska, 2008).

Other survivors of the Cryogenian glaciations were eukaryotes such as algae and amoebae, which diverged before the Cryogenian (Knoll, 1992, Butterfield, 2000, Knoll, 2014). Molecular clock studies indicate that plants, animals and fungi diverged from each other in the Mesoproterozoic at ~1 Ga (Doolittle et al., 1996, Wray et al., 1996, Wang et al., 1999).

Shirin Baydjanova
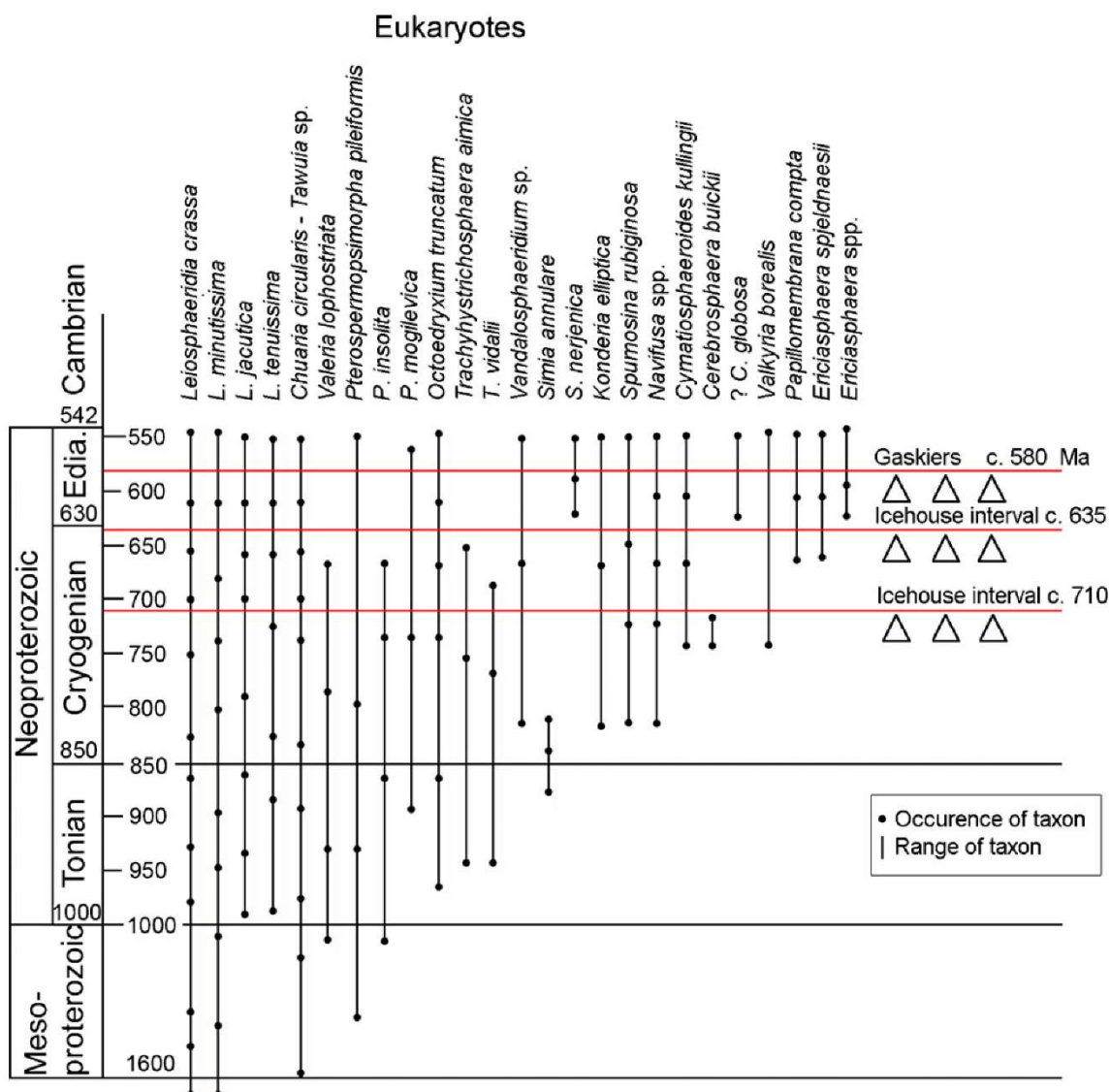
Figure 1.1.1. Range chart of eukaryotic species that survived the Cryogenian Period, and their approximate ages (Moczydłowska, 2008).

If the molecular clock estimates are correct, then animals should have existed before the Snowball Earth and probably have survived the glaciations (Corsetti et al., 2003, Xiao, 2004, Meert et al., 2011). The well-known Precambrian discoidal fossils of *Twitya* discs (found in the Twitya Formation, Canada, age constraint between Sturtian and Marinoan) have now been interpreted as stem-group cnidarians (Hofmann et al., 1990), meaning that stem-group sponges and possibly stem-group bilaterians existed before the Marinoan (Figure 1.1.2) (Xiao, 2004).

Shirin Baydjanova
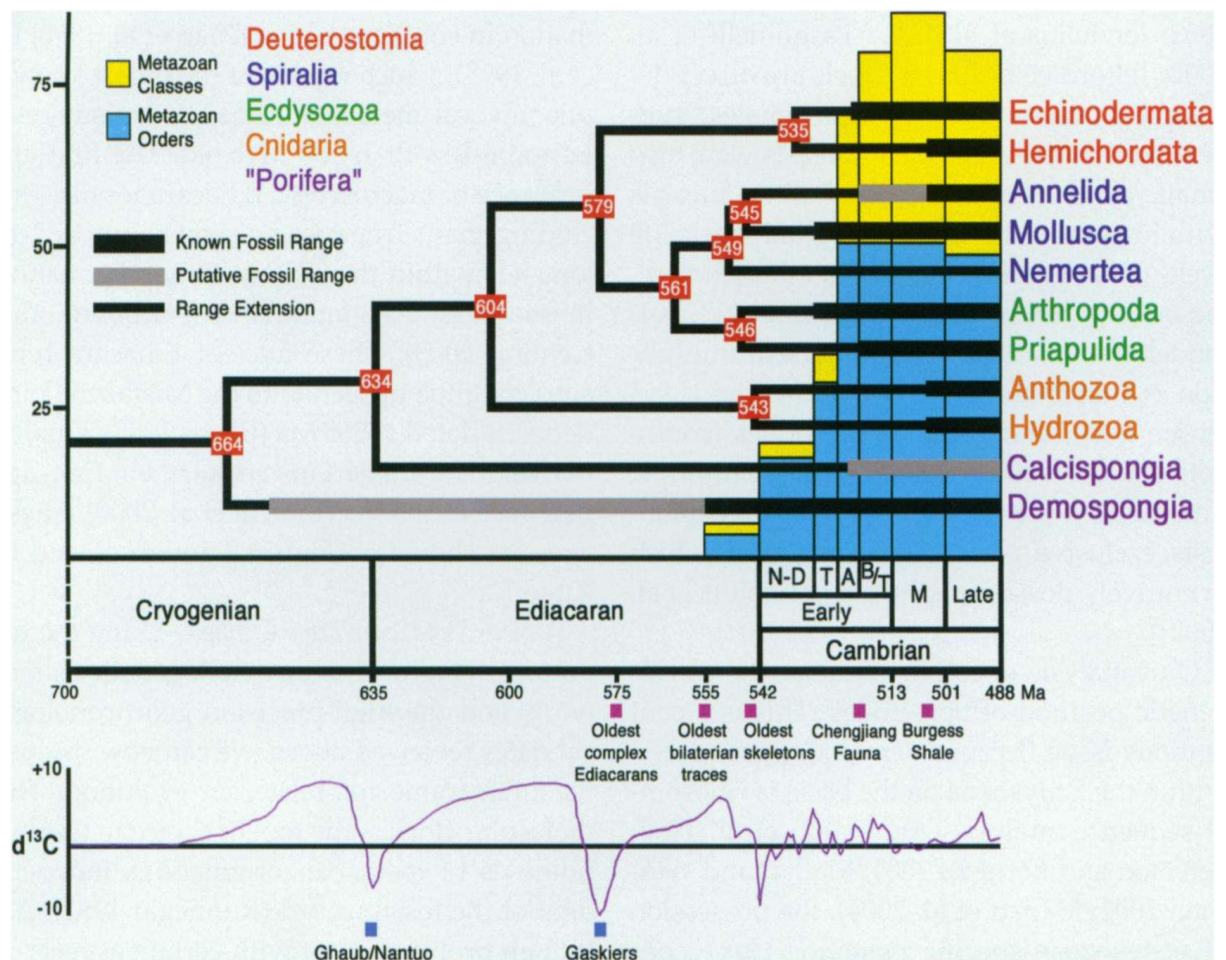
Figure 1.1.2. Appearance and evolution of animals by molecular clock estimation with carbon isotope curve (Knoll, 1999, Peterson et al., 2005).

The molecular clock studies have spurred many palaeontologists and geochemists to try to find an evidence of the proto-metazoa before the Ediacaran and even before the Cryogenian (Love et al., 2009, Maloof et al., 2010, Brain et al., 2012, Wallace et al., 2014, Yin et al., 2015).

1.2 Existing research

1.2.1 Fossil studies

There is evidence based on fossil findings and molecular clock studies that the proto-sponges (considered to be the first animals on Earth) evolved before and during the first Snowball Earth event (Love et al., 2009, Maloof et al., 2010, Yin et al., 2015). Others insist that the

Shirin Baydjanova

fossil findings could be explained by other organisms such as algae, protists, or microbial life (Corsetti et al., 2003, Bosak et al., 2011, Antcliffe, 2013).

The study made by Brain et al. (2012) claims to have found sponge fossils at a site located in Namibia, southern Africa. The succession of formations where these particular fossils have been found puts the timeframe between 760 Ma and 550 Ma (Figure 1.2.1).
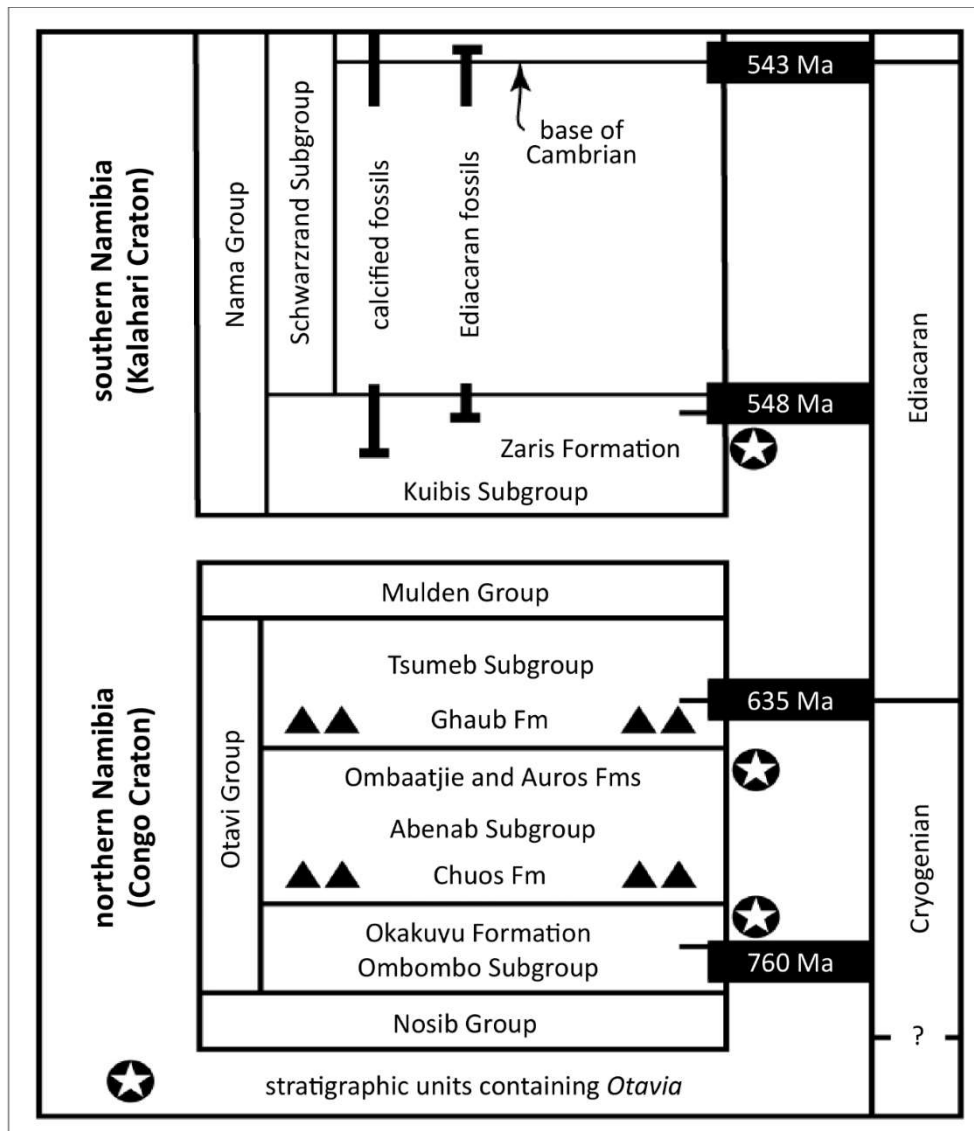
Figure 1.2.1. Stratigraphy of Namibian formations where the sponge fossils (*Otavia*) were found (Brain et al., 2012). Stars = fossils sites, triangles = glacial formations.

Two other studies found chambered structures that resemble sponges in two different formations in South Australia (Maloof et al., 2010, Wallace et al., 2014). The age of these

Shirin Baydjanova

formations correlates with the formations in Namibia, where the sponge fossils have been found (Figure 1.2.2).

Figure 1.2.2. Comparison of the Australian and Namibian formations where the fossils of sponges (chambered structures) have been found (Wallace et al., 2014). Blue = Sturtian glacial and cap dolomite formations, yellow = Marinoan glacial and cap dolomite formations, green = interglacial formations with chambered structures.

However, fossils from such old rocks are very scarce and not readily available for studies. Furthermore morphology alone might not provide assessment of lineage. Therefore, other methods, including the use of molecular sequence calibration as well as biomarker abundance and distribution can help trace the order of animal evolution (Wray et al., 1996, Kelly et al., 2011).

Shirin Baydjanova

1.2.2 Biomarkers and biomarker studies

Biomarkers are molecular fossils that come mostly from lipids (fats) of organisms. The biomarkers are relatively resistant to weathering, changes in pressure and temperature, and biodegradation (Peters et al., 2005).

A biomarker study of sedimentary rocks from the Huqf Supergroup, South Oman Salt Basin (~635Ma) found a biomarker called 24-isopropycholestane, which is a chemical compound produced by modern demosponges (the largest family of sponges that exists today) (Love et al., 2009). This study is significant in several ways:

1) There are no other fossils of sponges found that are older than the Cambrian. The demosponges have very small siliceous parts of their skeletons that are called "spicules" and these spicules are curiously absent from all Precambrian rocks. However, the study found fossilised steroids called "steranes"; hydrocarbon biomarkers of sponges in a 100 Ma succession of rocks in Oman.

2) The implications of the Oman findings are that the molecular clocks used by biologists as the start of the animal life on Earth could be pushed back by almost 100 million years and change our views on the life conditions during the Cryogenian Snowball Earth events. These findings also suggest that life is more resilient to harsh conditions than was previously thought.

However, it is not clear if these proto-sponges were restricted to one or two localities, or were more widespread. To find out, we need to analyse more rocks of approximately similar age that contain organic matter from several other localities.

1.3 Aims of the present study

The main aim of this study is to establish whether the samples of Cryogenian interglacial age from Australia and Namibia have been preserved well enough to assess hydrocarbons, and biomarkers. Another goal is to establish their thermal maturity. The rocks in this study are more than 500 Ma old and have been metamorphosed, however, it is not clear up to what temperatures they were heated. Extreme heating of ≥ 200 °C (metagenesis), prior to greenschist metamorphism, could result in the complete or partial thermal alteration of any

Shirin Baydjanova

organic matter suitable for geochemical analysis (Peters et al., 2005). To overcome this problem, other methods have been employed, such as:

1) SEM imaging (secondary electron (SE) and back-scattered electron (BSE)) to find the locations of kerogen/organic matter and to find out what minerals are associated with it;

2) Fluorescence microscopy studies to identify the morphologically-recognisable organic matter (it should fluoresce if not over mature);

3) Confocal Micro Raman spectrometry to assess the amount of kerogen-to-graphite conversion;

4) Fourier Transform Infrared Spectroscopy (FTIR) to check the type of carbonate matrix and the level of its dissolution after the acid treatment; to identify organic functional groups as well as to determine the maturity of the kerogen.

Another major aim of this study is to develop the extraction and processing techniques necessary to ensure that the samples are not contaminated and the organic matter present is indigenous.

Chapter 2. Geological settings of the samples

2.1 Sample localities

The Northern Adelaide Geosyncline in South Australia contains a sedimentary sequence that covers both the Sturtian and Marinoan glaciations, and the interglacial times in between. The Balcanoona Formation (Figure 2.1.1), which is a part of the interglacial succession, was a marine reef that has been dated at ~650 Ma. The shallower-water portion of the fossil reef consists almost entirely of stromatolites, while the deeper-water part contains abundant chambered calcified structures identified as possible sponge-like fossils (Figure 2.1.2) (Fromhold and Wallace, 2011, Hood et al., 2011).

Shirin Baydjanova
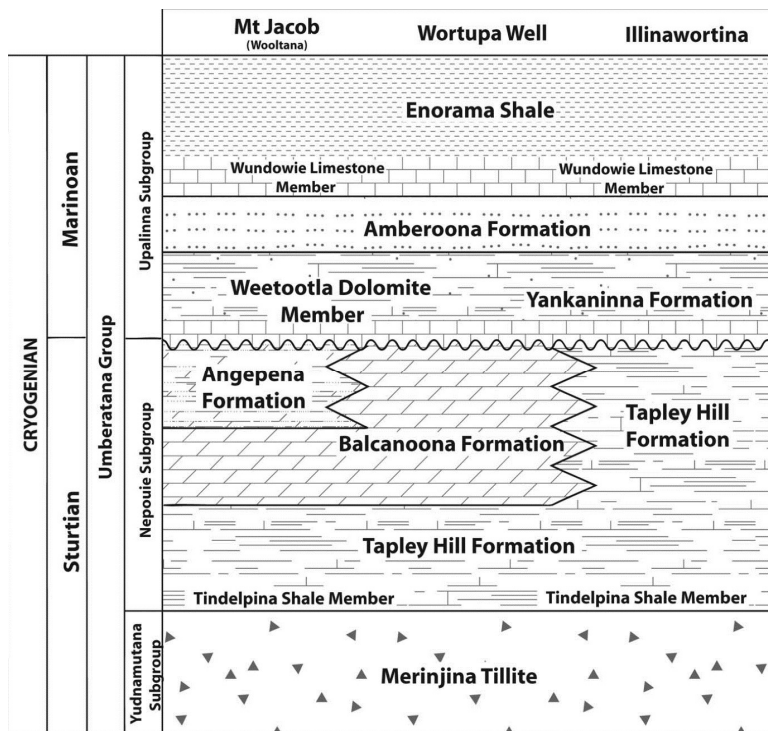
Figure 2.1.1. The stratigraphy and age of the Balcanoona Formation (Fromhold and Wallace, 2011).
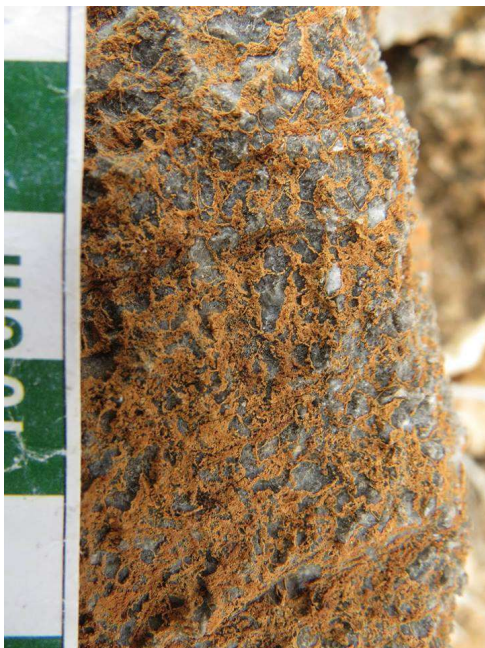
Figure 2.1.2. Possible sponge fossils in the Balcanoona Formation, northern Flinders Ranges, South Australia. Chamber walls (orange) and chamber fill (grey). Divisions in scale at left are 1cm. Photo courtesy of Prof Simon George.

Shirin Baydjanova

The chambered structures in Namibia (Figure 2.1.3) occur in the late Cryogenian strata of the Rasthof-Berg Aukas formations (lateral equivalents in the Kaokoveld and Otavi Mountainland, respectively) (Hoffmann and Prave, 1996), and the Gauss Formation (Otavi Mountainland and Fransfontein Ridge regions, ~746-635 Ma) (Pruss et al., 2010). The Namibian rocks are very close in age to the South Australian rocks, and are similar in structure (in that they have reefal growth frameworks). The Rasthof Formation is divided into three informal units from base to top: the basal cap dolostone (consistent with Sturtian cap dolomites from elsewhere), the microbial member, and the epiclastic member (Figure 2.1.4). The chambered structures are abundant in the microbial member of the succession, however, they are also widespread both in the stromatolitic part of the microbial member and in the non-stromatolitic epiclastic member (Wallace et al., 2014). The main difference between the Australian and Namibian rocks is the greater abundance of carbonates in the Namibian formations.

Shirin Baydjanova

Figure 2.1.3. Chambered structures in two samples of the Rasthof Formation, Namibia. Top, Bull; bottom, Huab North 2 (HN2). Samples provided by Prof Malcom Wallace (University of Melbourne); photo by author.

Shirin Baydjanova
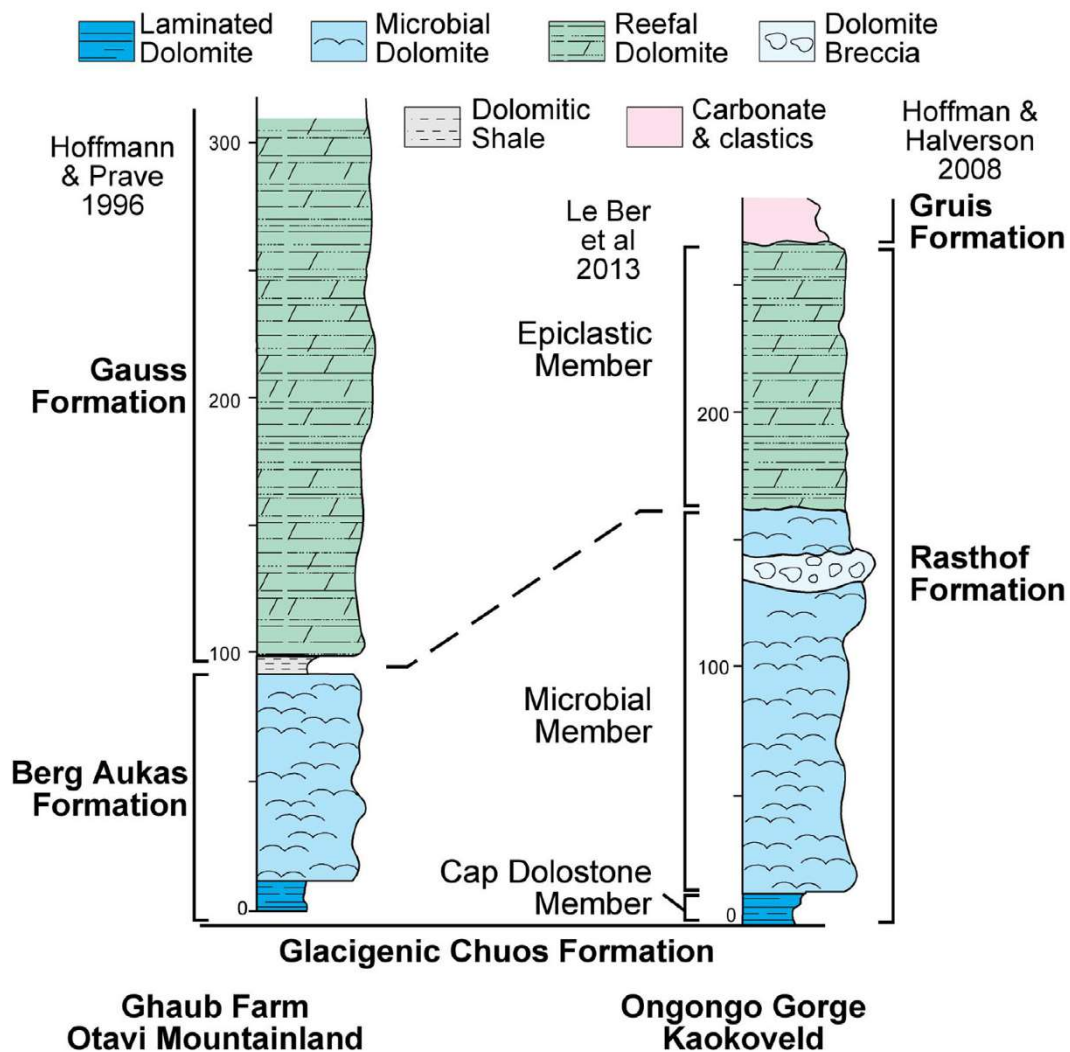
Figure 2.1.4. Stratigraphy of Rasthoff Formation (Wallace et al., 2014).

The Amadeus Basin is another location in Australia with sequences of formations from before the Sturtian to the Early Carboniferous (Figure 2.1.5). These are very promising rocks to contain traces of complex organisms, as they are known for their richness in organic matter. The formations of interest for this study are the Cryogenian Aralka Formation that lies on top of the Sturtian Areyonga Formation, and the corresponding Inindia Beds Formation that have been identified as potentially gas and oil producing rocks (Figure 2.1.5) (Munson, 2014). Jarrett (2014) showed that the Amadeus Basin rocks are abundant in biomarkers, including steranes, however, the study did not focus on the sponge biomarkers. Nevertheless, this study also showed that the Cryogenian rocks of low thermal maturity do exist.

Shirin Baydjanova
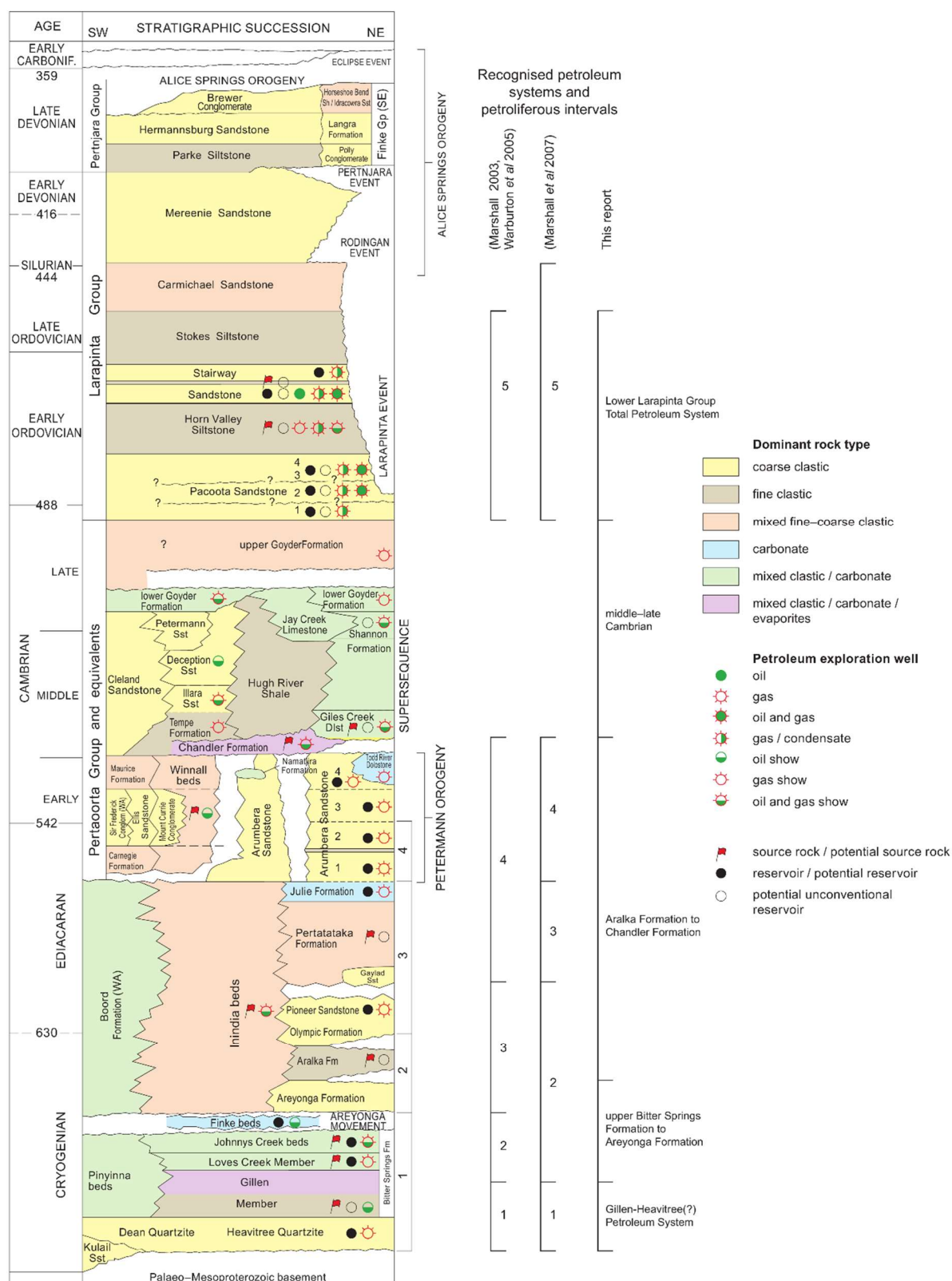
Figure 2.1.5. The Amadeus Basin stratigraphy (Munson, 2014).

Shirin Baydjanova

In this study only samples from the Northern Flinders Ranges and from the Congo Craton were analysed due to the shortage of time and limited funding.

2.2 Thermal maturity

2.2.1 Samples from the Tapley Hill and the Balcanoona Formations

The Adelaide Fold Belt, or the Adelaide Rift Complex, in the northern Flinders Ranges consists of the Neoproterozoic and Cambrian sedimentary rocks that were variably metamorphosed during the Delamerian Orogeny (~500 Ma) (Paul et al., 1999). The Adelaide Fold Belt has four structural provinces: the Adelaide Fold-Thrust Belt in the south, the Nackara Arc in the east, the central Flinders Ranges in the mid-north, and the northern Flinders Ranges in the far north (Figure 2.2.1).
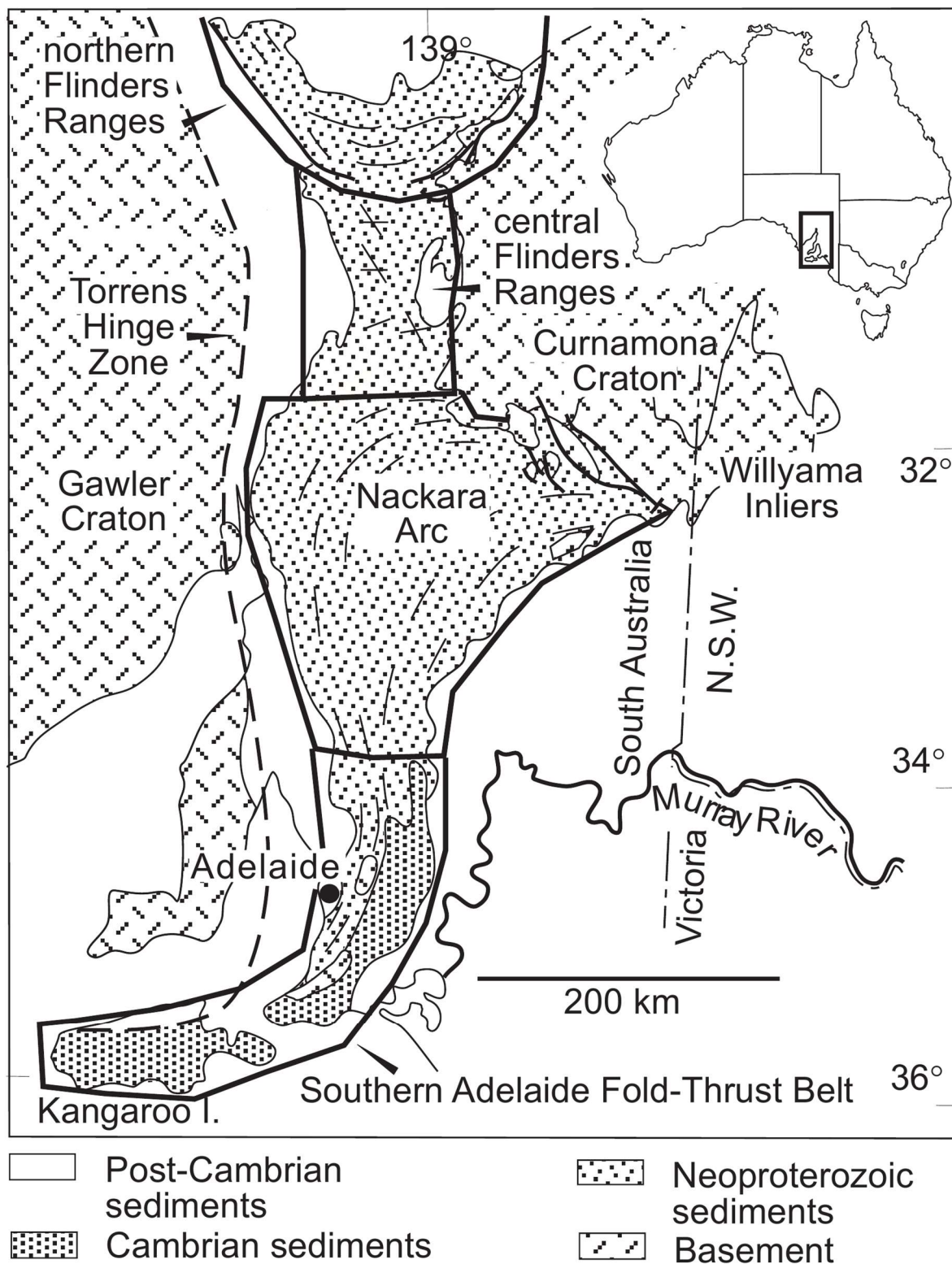
Figure 2.2.1. Adelaide Fold Belt provinces (Paul et al., 1999).

The samples for this study have been collected in the northern Flinders Ranges from the Umberatana Group (the Tapley Hill and the Balcanoona Formations). Therefore, the maturity parameters are relevant only for this part of the Adelaide Fold Belt.

The studies of the Neoproterozoic sequence of the Adelaide Rift Complex by McKirdy et al. (1975), McKirdy et al. (2001) showed that the regional metamorphism increases from west to east across the Complex. It was also noted that the original isotopic composition of organic matter was preserved. The study revealed a positive gradient of $\delta^{13}C_{carb}$ (from +1‰ to +9‰) starting from the Tindelpina Shale (that overlies the Sturtian cap carbonates) through the Tapley Hill Formation and the Brighton Limestone/Balcanoona Formation up to the Etina Formation. This observation is very important for the current study, as the samples were collected from the upper Tapley Hill Formation and from the Balcanoona Formation.

The study by Bons et al. (2009) argued that metamorphic temperatures near Oppaminda Creek (Tapley Hill Formation) did not exceed 200°C. However, further north towards the Mt. Painter Inlier, the metamorphism reached the amphibolite facies. The study also found fossils of unknown origin (possibly microbes) in the calcite veins from Oppaminda Creek, Northern Flinders Ranges, South Australia.

Paul et al. (1999) also agreed that the majority of the Adelaide Fold Belt experienced the degree of metamorphism up to the biotite grade, while the grade in the northern province was up to the sub-greenschist facies. They agreed with Bons et al. (2009) about the higher metamorphic grade of the Mt. Painter and Mt. Lofty areas.

The Tapley Hill Formation is a calcareous finely laminated siltstone that was most likely deposited in a calm deep-water environment favourable for organic matter preservation (Total Organic Carbon (TOC) = 0.1 – 1.2 %) (McKirdy et al., 2001). The carbonates in this formation are mostly dolomicrite (up to 20%) that could have been directly precipitated from Mg-rich diapirically-derived salts. There is a negative correlation between the TOC and $\delta^{13}C$ values for both organic carbon and carbonate, with TOC increasing as $\delta^{13}C$ decreases. Low values of $\delta^{13}C_{org}$ could be explained by the differences in palaeobathymetry as the benthic biomass is usually more depleted in ^{13}C than its planktonic equivalent. The ^{34}S in the lower Tapley Hill shows an enrichment ($\delta^{34}S$ = +9 to +40‰) that could be explained by bacterial activity (McKirdy et al., 2001).

Shirin Baydjanova

Giddings et al. (2009) agree with McKirdy et al. (2001) that the Tapley Hill Formation was deposited in the deep-water environment compatible with marine transgression after the end of the Sturtian glaciation.

The Balcanoona Formation was a marine reef that shows distinct parts similar to modern reefs such as back-reef (platform), reef-margin, and fore-reef (slope) (Giddings et al., 2009). The reef structure can be divided into the stromatolitic and non-stromatolitic frameworks with large amounts of both present as allochthonous blocks within the Tapley Hill Formation (Hood et al., 2011). It seems that during the reef's life the change in environmental conditions led to the erosion of the reef margin and these allochthonous blocks are the debris flow deposits. Interestingly, the reef complex itself is mostly dolomitic while the blocks within the Tapley Hill Formation are a mix of limestone and dolomite. Either the shales have protected the blocks from dolomitisation fluids, or the dolomitisation was due to organic processes. The latter hypothesis is supported by carbon isotope data where the $\delta^{13}C$ values for dolomites are slightly lower than the $\delta^{13}C$ values for limestone.

2.2.2 Samples from the Rasthof Formation

The Neoproterozoic Otavi Group (Figure 2.2.2) of the Pan-African Damaras Fold Belt in Namibia (~750- 450 Ma) was deposited on a rifted passive margin of the southern Congo Craton (Kroener, 1982, Hoffman, 2002, Pruss et al., 2010, Le Ber et al., 2013).

Shirin Baydjanova
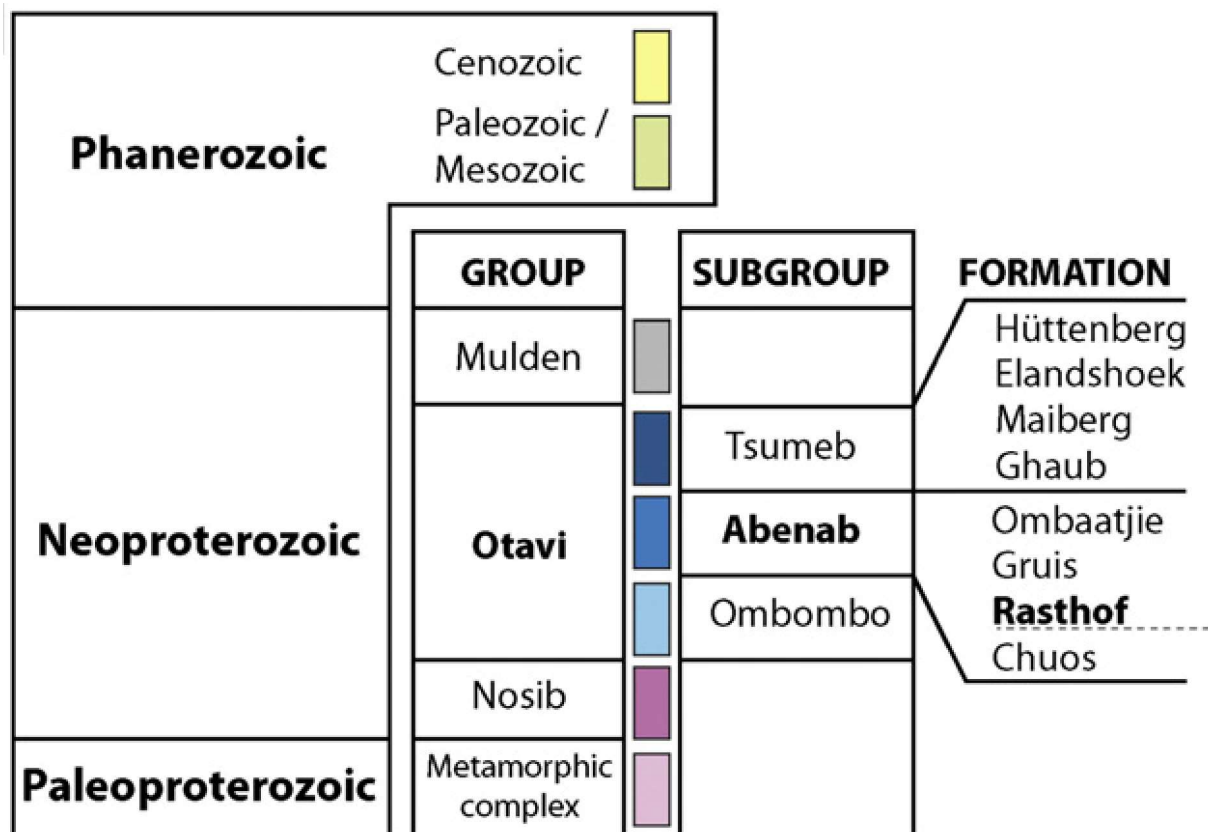
Figure 2.2.2. Stratigraphy of the Otavi Group (Le Ber et al., 2013).

The initial rifting led to the deposition of the Nosib Group while later subsidence and transgression facilitated the development of a carbonate platform on which the Otavi Group had accumulated in a thick sequence (Figure 2.2.3) (Kaufman et al., 1991).

Shirin Baydjanova

LEGEND

- Karo & Recent
- Nama Group
- Syn-and post-tectonic granitoids
- Pre-tectonic granitoids
- Volcanic rocks
- Metasediments with structural trends
- Pre-Damara basement
- Fault, thrust
- O.L. Okahandja lineament
- M.A. Matchless amphibolite belt
- Approximate boundary miogeosyncline / eugeosyncline

0   50   100 km
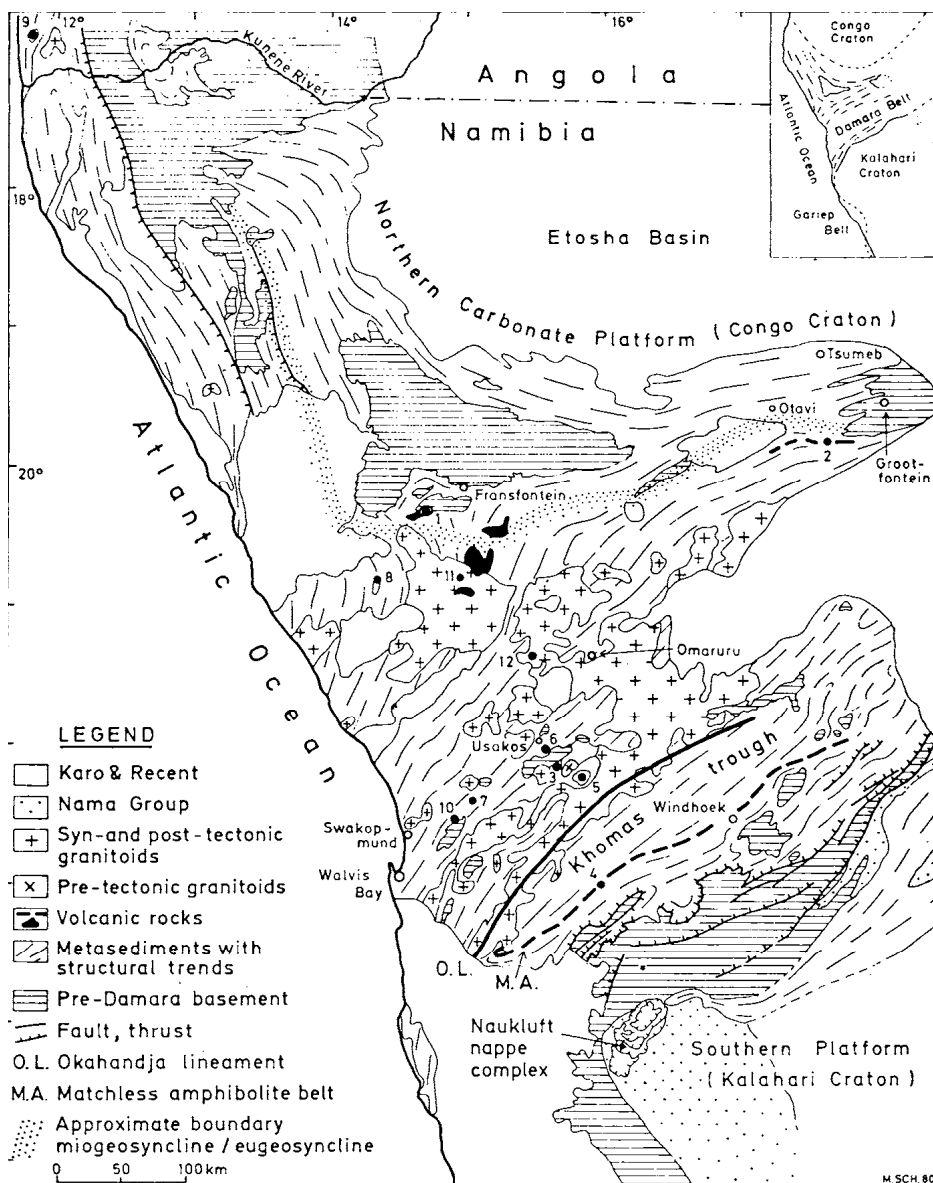
Figure 2.2.3. A simplified map of major structural features of the Damara Fold Belt (Kroener, 1982).

There is evidence of the episodic occurrence of igneous rocks related to the Neoproterozoic continental rifting that occurs for 400 km along the northern margin of the Damara Fold Belt (Hoffman et al., 1996). Their highly localised distribution and large thickness suggest an association with tectonic extension or/and cauldron-subsidence structures. This igneous activity coincided with continental break-up at the southern margin of the Congo Craton (Hoffmann, 1994) (Figure 2.2.3 inset). As a result of these perturbations, the rocks of the Rasthof Formation are most likely metamorphosed.

Shirin Baydjanova

The Rasthof cap-carbonate sequence is exposed at the Huab ridge and the Hoanib shelf locations. In the Otavi Mointains the Aukas-Berg Formation is the equivalent to the Rasthof Formation (Hoffmann and Prave, 1996). On the Hoanib shelf the basal cap dolostone member has $\delta^{13}C$ values from -4.5‰ to -2.0‰; there is an increase to 0‰ at the top of this unit and up to 5‰ in the microbial member (middle part of the formation) and decreases back to 0‰ in the upper epiclastic member (Hoffman, 2002). This variation in $\delta^{13}C$ suggests that the microbial member was deposited in a restricted basin with a depth of ~200 m (Figure 2.1.4). The folded "roll-up" structures of the microbial mats and the presence of syn-sedimentary breccia implies either fluid or gas escape from the bottom of the basin (Hoffman, 2002). On the Huab ridge and in the Otavi Mountains the $\delta^{13}C$ profile is similar to the Hoanib shelf (Hoffmann and Prave, 1996, Hoffman, 2002).

The study by Kaufman et al. (1991) also agrees that the extensional basins could have a hydrothermal input. They pointed out that the formation of iron-rich deposits in the underlying Chuos tillite is a good indicator of iron-rich hydrothermal fluids. Indeed, Hoffman (2002) noted that the Chuos Formation is so haematite-rich that the base of the Rasthof cap carbonate is discoloured by haematite and the Rasthof dolomites are also Fe-rich. In contrast to Hoffman (2002), the investigation by Kaufman et al. (1991) of $\delta^{13}C$ and TOC of Aukas-Berg Formation dolomicrites reports whole rock $\delta^{13}C$ values of 2.1 - 3.1‰ and TOC values of 0.2 - 0.4 mg C/g.

Pruss et al. (2010) agreed with the deeper water environment of the microbial member deposition with a fluid escape from the dykes, which could have been formed due to the tectonic activity. Le Ber et al. (2013) on the other hand, argued that the microbial member was deposited in a much shallower environment than was previously thought.

Chapter 3. Methods

3.1 Extraction methods and procedures

3.1.1 Contamination control

Contamination is a major problem when working on the organic geochemistry of lean Precambrian rocks (Hoering, 1965, Oehler, 1977). The goal is to reduce the contamination that can come from many different sources in the lab as well as during sampling and storing

Shirin Baydjanova

(Illing et al., 2014). The first step in achieving that was to ensure that the instruments and methods used in this study were not contributing to the contamination. All laboratory equipment was tested for traces of organic compounds in the first month of this nine month study. As a result, the Accelerated Solvent Extractor (ASE) and the rotary evaporator Rotavapor R-210, BUCHI were eliminated from the analytical protocol as they are major sources for contamination, mostly because these instruments are shared by all lab workers and often used for an extraction and reduction of organic-rich samples (French et al., 2015, Hoshino et al., 2015, Hoshino and George, 2015).

Other possible sources of contamination were the glassware, tweezers, spatulas, solvents, organic residues on the rock surfaces, the rock saw, and the ring-mill. The glassware was soaked overnight with Decon 90, then washed with filtered water, and combusted at 400°C for 3 hours, which had proven to be enough to eliminate any possible contamination (Hoshino, 2015). However, the configuration of the round-bottom flasks (RBFs) tends to help to retain some organic residues, so they were also not used in this study. Similarly, all pipettes and an aluminium foil used in this study were combusted the same way.

The tweezers and spatulas were washed and sonicated with Dichloromethane (DCM) for 5 min before each use. The tungsten carbide ring-mill crusher (Rocklab) (Figure 3.1.1) was washed manually and then rinsed mechanically several times with methanol, then a mix of DCM and methanol (9:1 v/v), and then just DCM. Each time the solvent was discarded, except for the last wash when it was collected, spiked with an internal standard, and analysed by gas chromatography-mass spectrometry (GC-MS) to check the contamination level. Obviously, it is not possible to completely eliminate the contamination, so the standards were assigned as 100% and any organic contamination of $\leq 5\%$ relatively to the standard was deemed suitable to allow analysis of samples to proceed.

Shirin Baydjanova

Figure 3.1.1. The tungsten carbide ring-mill crusher.

Another major source of contamination was the rock saw. Due to its size it was impossible to sterilise it by heating as was done for the glassware, or by sonication with a solvent as was done for the tweezers and spatulas. Therefore, it was used as it was, however, for the consistency of the experiment, all rocks were cut with the same saw and tap water cooling, thus under the same conditions.

Before cutting the rocks were sonicated with a mixture of DCM and methanol (9:1 v/v) to remove organic contamination. Then all outer surfaces were cut off and the inner parts of the rocks were cut to approximately 1-1.5 cm cubes.

After the rock cutting and before the crushing in the ring-mill, the rock cubes (Figure 3.1.2) were sonicated in DCM four times, with the solvent discarded after each sonication except for the last. After the fourth sonication, the solvent was collected and analysed by GC-MS and then compared with the extracted sample results to ensure that the compounds from the extract did not come from the outside surfaces. Other blanks that were used in this study include DCM, HCl, and a basalt blank.

Shirin Baydjanova

Figure 3.1.2. Rock cubes after cutting (sample Bull). The sizes of the cubes are ~ 1cm^3.

The solvents that were used in this study were mostly DCM and methanol and these also may contain some organic compounds and thus can be regarded as a contamination source. Several brands of DCM and methanol were tested (Scharlau, Macron, Lichrosolve, RCI LabScan, and Honeywell Burdick & Jackson). The Honeywell Burdick & Jackson was shown to be the best and was used for the whole study. However, as the contamination level changes from batch to batch, one bottle from each new batch was tested by GC-MS analysis and results were compared with the samples results. The majority of contaminants were low-molecular weight n-alkanes and siloxanes.

Internal standards were diluted in the DCM as described above, and as a result can contain the same contamination compounds as the solvent. In addition, the standards tended to degrade with time even if stored in a dark cold place, so repetitive testing of the standards was also performed and, if needed (poor peak resolution), a new one was made. The standards used in this study were: 1,4-Dichlorobenzene; Anthracene-d$_{10}$; Tetracosane-d$_{50}$; and p-Terphenyl-d$_{14}$.

The acid used in the study was 36% HCl, produced by RCI LabScan. The purity checks showed that it contained quite high amount of n-alkanes, thus the acid was cleaned several times by solvent-back extraction and tested for cleanliness. The acid was used only after the level of n-alkanes became significantly lower.

Shirin Baydjanova

3.1.2 Solvent extraction techniques

Three types of solvent extraction techniques were tested in this study:

- Bitumen I extraction method – solvent extraction by sonication.
- Bitumen II extraction method – partial dissolution of the rock powder with acid, followed by solvent extraction by sonication.
- Third method – solvent extraction with sonication on both undissolved and acid dissolved rocks using different mixes of solvents (experimental).

3.1.2.1 Bitumen I extraction method

In bitumen I extraction method, 30 g of rock powder (where possible) were extracted by sonication in an ultrasonic bath (Unisonics N1984) three times for 10 minutes using 50 to 100 mL of DCM/MeOH (9:1 v/v) for the first two sonications. Between the sonications the samples were stirred with a glass rod and left to stand for 10 min (covered with foil). After the second sonication the supernatant was collected and centrifuged (centrifuged by Hermle Z206A) at 2500 rpm for 5 minutes to help the suspended rock particles to settle. For the third sonication 30 mL of DCM were added to the samples and they were sonicated another 10 minutes to recover the remainder of the organic compounds. Then, the solution containing extractable organic matter (EOM) was added to the first collected aliquot, centrifuged if needed and reduced on a hot plate (40°C) under a gentle continuous nitrogen gas stream until only ~ 10 mL of the solvent with EOM was left.

In cases where the EOM solution still contained some very fine particles, the solution was filtered through a silica column (Pasteur pipette, plugged with glass wool and topped with 45 mm of dry activated silica gel). Silica gel (silica gel 60, 0.063-0.200 mm, Merck) was previously activated and cleaned by combusting it in the same conditions as the glassware (400°C for >3h). Then the sample was reduced to ~250 μL, and spiked with the standards (1 mL containing 50 ng of each standard) for gas chromatography–mass spectrometry (GC-MS) analysis. After an unexplainable disappearance of tetracosane after the first sample run, the amount of this hydrocarbon was changed from 50 ng to 500 ng. Column fractionation of the EOM was not performed to prevent the loss of hydrocarbons as the rocks are extremely organic-lean (~1–2 mg of EOM/g of rock powder).

Shirin Baydjanova

3.1.2.2 Bitumen II extraction method

Bitumen I extraction method did not yield high enough amounts of the compounds to analyse. This may have been due to the fact that the carbonate matrix isolates organic matter (OM) and prevents the OM extraction (Dutkiewicz et al., 2004). The FTIR measurements of un-extracted and extracted powder showed almost no difference (Figure A.1), which supported this hypothesis. Calcite and dolomite have peaks in four regions: 1420 – 1450, 870 – 890, 700 – 720, and 1000 – 1100. Calcite has a distinct peak at ~ 712 cm^{-1} and dolomite – at ~ 728 cm^{-1} (Gunasekaran et al., 2006). The absorption bands at 3020, 2626 and 730 cm^{-1} are characteristic of dolomite only (Ji et al., 2009). For a description of the method and the parameters used see chapter 3.2.2 below.

The bitumen II extraction method was similar to that described in Nabbefeld et al. (2010) with some modifications. To dissolve the carbonate matrix, firstly 90 mL of 6% HCL acid was used on the AK005 and AK019 samples (in two steps, 60 mL first and then 30 mL). After the effervescence ended, the samples (covered with foil) were heated on a hot plate (70°C) until the dissolution completely stopped (Figure 3.1.3). The samples were then washed with 500 mL of MilliQ water six times. To prevent the loss of low molecular weight fractions that formed on the top of the sample-acid-water mix, the solution was washed via glass funnels that were plugged with glass wool, using activated silica. After the samples were air-dried whilst covered with foil, they were extracted together with the silica, using the same technique as described in section 3.1.2.1.

Figure 3.1.3. AK005 and AK019 samples on a hot plate after addition of 6% HCL.

Shirin Baydjanova

This method proved to be more effective in the extraction of the hydrocarbons than the first. However, following FTIR analysis showed that some of the carbonate matrix still remained (Figure A.2). Note the higher absorption peaks in the sample treated with 36% HCl (blue line).

Thus, it was decided to use 36% HCl for all the other samples including the first two (AK005 and AK019). The previously acid digested samples that did not show any more reaction with 6% HCL, nevertheless showed a very strong reaction when 36% acid was added (Figure 3.1.4).

Figure 3.1.4. Samples AK019 (left) and BAO-2A (right) treated with 36% HCl.

After acid digestion and solvent extraction by sonication, the EOM was treated with activated copper (metal turnings, TG, Chem-Supply) to remove any elemental sulphur. The copper was activated with 36% HCl followed by washing three times each with methanol and DCM, respectively. About 5 g of activated copper was used for each sample, except for sample BAO-2A, which required 15 g of activated copper due to a higher elemental sulphur content. The copper particles were then removed by decanting the EOM solution. The samples were again reduced to ~250µL and spiked with the standards.

3.1.2.3   Third solvent extraction method

The third solvent extraction method was performed as described by Mastandrea et al. (2011). In short, the acid digested and non-digested powders were extracted by sonication 3 times (30 minutes each) using a mix of methanol and DCM in equal volumes (1:1 v/v). This type of solvent extraction was mostly done for the FTIR analysis to help to determine the thermal maturity of the OM. However, it produced a bright yellow-green supernatant that was fractionated into polar and hydrocarbon (HCs) fractions (*n*-hexane and DCM (4:1 v/v) to elute the HCs and methanol and DCM (1:1 v/v) to elute polars), and then the HCs were also analysed by GC-MS.

Shirin Baydjanova

3.2 Analytical methods and data processing

3.2.1 Secondary Electron microscopy (SEM)

Polished thin sections were prepared for petrographic examination, fluorescence microscopy, SEM, and Raman spectroscopic investigations. After the petrography and fluorescence examination it was concluded that the organic matter is, probably, too small to be detected by these means. The bright fluorescence of calcite also was a hindrance. As the result, the Cameca SX-100 electron microprobe with Zeiss EVO MA15 Scanning electron microscope (with Oxford Instruments Aztec Synergy EDS/EBSD) was used to locate the OM, determine the size of the OM spots and to map the best sites for the Raman spectrometry. Prior to analyses, the thin sections were coated with a thin carbon film ≤ 10 Å in thickness. SEM data is considered to be semi-quantitative in this study as the carbon coating thickness for the samples measured and for the standards used was different, which influences the quality of the data.

3.2.2 Fourier Transform Infrared Spectroscopy (FTIR)

FTIR is a technique for the identification of organic groups and minerals (Mastandrea et al., 2011). FTIR is complementary to Raman spectroscopy and GC-MS. In this study a Thermo Nicolet iS10 ATR-FTIR (Nicolet, Ma, USA) was employed. The spectra were acquired in a wavenumber area between 4000 and 500 cm^{-1} with 64 accumulations and a spectral resolution of 4 cm^{-1} wavenumbers. The background was corrected in air every 30 minutes. Data acquisition and spectra treatment were carried out with the Omnic Specta Software (Thermo Scientific). All six samples were analysed repeatedly before and after extraction to check if any hydrocarbons were extracted after bitumen I extraction, and how much of carbonate matrix was destroyed after bitumen II extraction.

3.2.3 Confocal Micro Raman spectrometry

Raman spectra of carbon material appear to be sensitive to different metamorphic grades, thus can be used to estimate the degree of metamorphism (e.g. Beyssac et al., 2002). The organic matter usually shows a Raman spectrum for structurally disordered carbon, while well-ordered carbon (or true graphite) indicates that the sample had been subjected to high-temperature processes and, possibly, also high pressures (e.g. Pasteris and Wopenka, 2003).

Shirin Baydjanova

In this study a JY Horiba LabRam Evolution high resolution confocal Raman Spectrometer with two lasers, equipped with a Si-based charge-coupled device (CCD) detector (Peltier-cooled), an integrated Olympus BX41 optical microscope and an automatized x–y stage was used on standard petrographic thin sections. The 532.21-nm line of a frequency-doubled Nd:YAG laser was used for excitation with a laser spot size of ~ 5x5μm, using a 50x long-distance objective (numerical aperture 0.55) and a slit width of 100 μm. The scattered light was dispersed by a grating with 1800 grooves/mm or 600 grooves/mm depending on the measured range. Spectra were calibrated using the 520.5 cm^{-1} band of a silicon wafer.

Acquisition time was 20 s with accumulations of 10 spectra for each site. Data acquisition and spectra treatment were carried out with the commercially available program LabSpec v6 (JY HORIBA). The focus of this study was on the first-order region (1200-1700 cm^{-1}) as there was no variability observed of the second-order bands (2400-3200 cm^{-1}) between the samples. The OriginPro 2015 (OriginLab) software was used to determine the peak position, integrated area, and band width (full width at half maximum, FWHM). The measurements were tested for heterogeneity on samples AK005 and AK019 (analysis of several different grains in the same sample), and for reproducibility on BAO-2A (repeated analyses of the same spot). Other samples were not analysed extensively as the SEM examination failed to find many/any spots with the organic matter.

3.2.4 Gas chromatography – mass spectrometry

Gas chromatography and mass spectrometry (GC-MS) analyses were carried out on an Agilent GC (6890N) coupled to an Agilent Mass Selective Detector (5975B) with the following parameters:

Column	Inlet	Oven	Carrier gas
J&W DB5MS	Initial 35 °C / 3 min	Initial 35 °C / 4 min	Helium (He), constant flow 1.5 ml/min
length 60 m	Final 310 °C / 0.5 min	Final 310 °C / 40 min	Pressure 22.48 psi
inner diameter 0.25 mm	rate 700 °C / min	rate 4 °C / min	Purge flow: 200 mL / min
film thickness 0.25μm			Purge time: 4.00 min
			Total flow: 204.0 mL / min

Shirin Baydjanova

The MS data were acquired in full-scan (m/z 50-550) and single ion monitoring (SIM) modes. 1µL of the EOM solution was injected for each mode.

The hydrocarbons were analysed with Agilent Mass Hunter Qualitative Analysis (vB.06.00) and Agilent MSD ChemStation Data Analysis software. Hydrocarbon identification was based on comparison of relative GC retention times and mass spectra with those previously reported.

Chapter 4. Results

4.1 SEM analyses

4.1.1 Australian samples from the Tapley Hill and Balcanoona formations

Samples AK005 and AK017 are siltstones from the Tapley Hill while sample AK019 is an allochthonous block from the Balcanoona Formation that is partially dolomitised limestone. The samples were only thinly coated with carbon (≤ 10 Å) prior to analysis, so it was possible to identify small disseminated amorphous and/or structured spots of OM not bound to the carbonate matrix (Figure B.1; Figure B.2; Figure B.3).

4.1.2 Namibian samples from the Rasthof and Berg-Aukas formations

The samples BAO-2A, Huab North 2, and Bull were reported to be composed mostly of dolomite with a greater abundance of carbonates than the Australian samples (Wallace et al., 2014). Distinct OM patches as in the Australian samples were not found during SEM imaging. However, it was clear that some OM is included in the carbonate grains as those grains were visually different (darker) from other "more pure" carbonates that do not contain OM (Figure B.4). Spot SEM analysis confirmed this hypothesis.

Calcite and dolomite have distinct compositions (Table 4.1.1). Dolomite contains ca. 22 wt% MgO (Mg/Ca is ~ 1.38) and the CO_2 concentration is ~ 44 wt% - 48 wt% (Deer et al., 1992). SEM/EDS measurements were used to identify the phases by the Mg/Ca ratio of the carbonate and the OM by elevated C concentrations due to extra thin coating with carbon.

Table 4.1.1. Typical calcite and dolomite compositions (Deer et al., 1992).

Calcite	CaO ~ 56.0 wt%	CO_2 ~ 44.0 wt%	
Dolomite	CaO ~ 30.4 wt%	CO_2 ~ 47.7 wt%	MgO ~ 21.9 wt%

Thus, the ratio of Mg/Ca is ~ 1.38 and the CO_2 contribution is ~ 44% - 48%. If the spot analysis showed elevated carbon (>50%), it was considered that the carbon grains contained some OM.

4.2 FTIR analyses

FTIR analysis is a relatively cheap and fast method to determine the carbonate mineralogy. Apart from a possibility to analyse a rock powder, EOM also can be analysed by FTIR. In this study FTIR analyses were carried out on the non-extracted powder and compared to the FTIR analyses of limestone by Reig et al. (2002). This was done with the aim to find out which samples are closer to a limestone and which are mostly dolomite or a mix of both (Figure 4.2.1).

Shirin Baydjanova
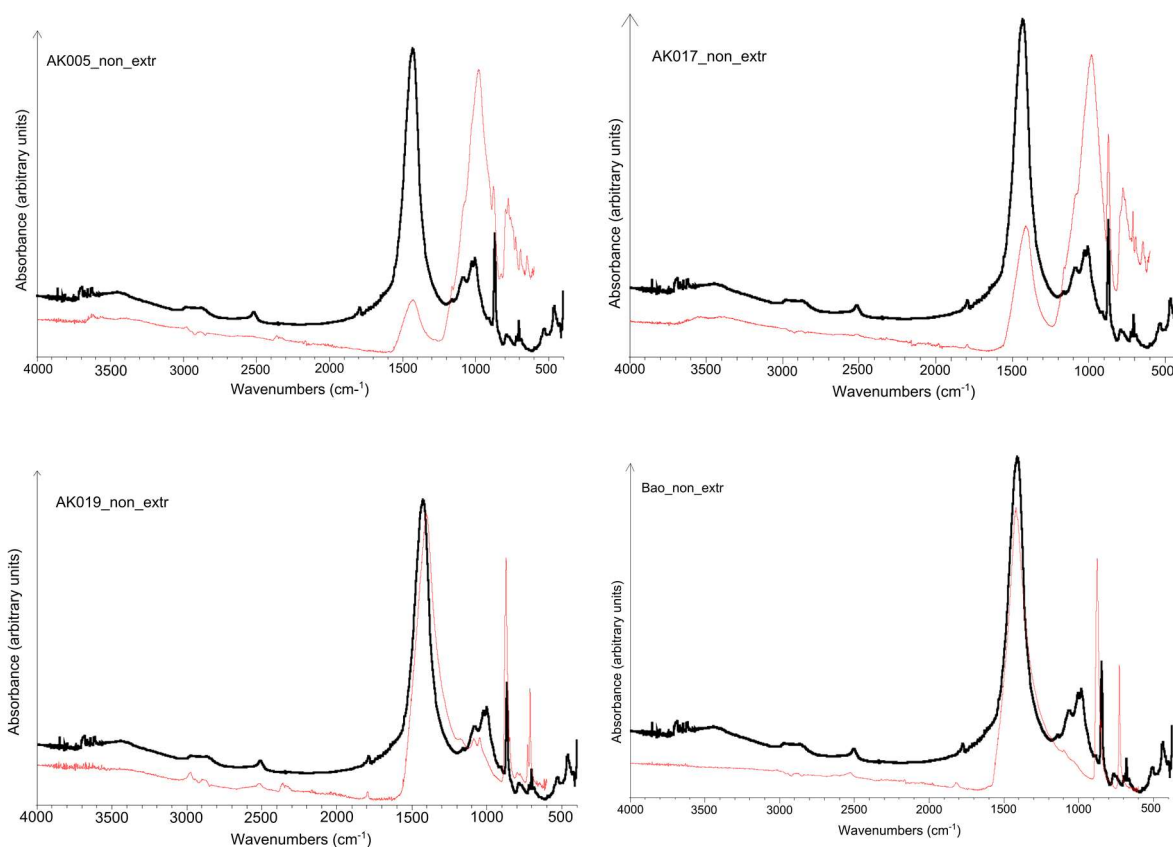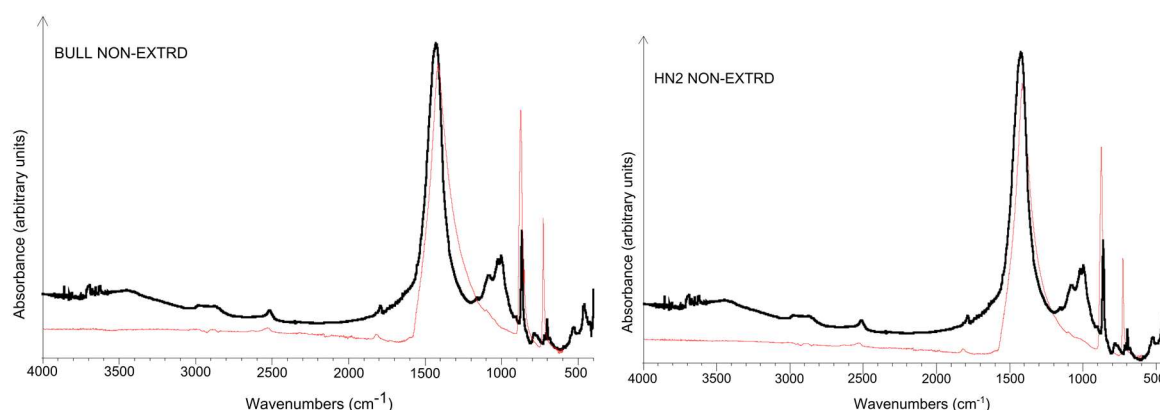
Figure 4.2.1. FTIR spectra of the Australian (AKxxx) and Namibian (Bao, Bull, and HN2) samples in red compared with spectra for limestone by Reig et al. (2002) (black line). The names of the samples are in the top left corner.

Analysis of the powder and the supernatant extracted from the rock-powder treated with 36% HCl was performed as described in Mastandrea et al. (2011) (Figure 4.2.2). Spectra of undissolved carbonate matrix and OM can overlap in the FTIR analysis and thus, the OM needs to be extracted so the interference is removed. This is especially important in the organic lean samples. Another convenience of this type of analysis is the possibility to distinguish organic and inorganic carbon.

Due to the changes in kerogen during thermal maturation, the FTIR spectroscopy on extracted OM can measure the shifts of several bands. For example, aromaticity (ratio of aromatic to aliphatic absorption) increases with thermal maturity (Mastandrea et al., 2011).

Lis et al. (2005) calculated FTIR parameters for aromaticity and used them as a proxy for thermal maturity determination (Figure 4.2.3). The 3100-3700 band functionality is not known, however, it is clear that the band becomes more pronounced with an increased thermal maturity.
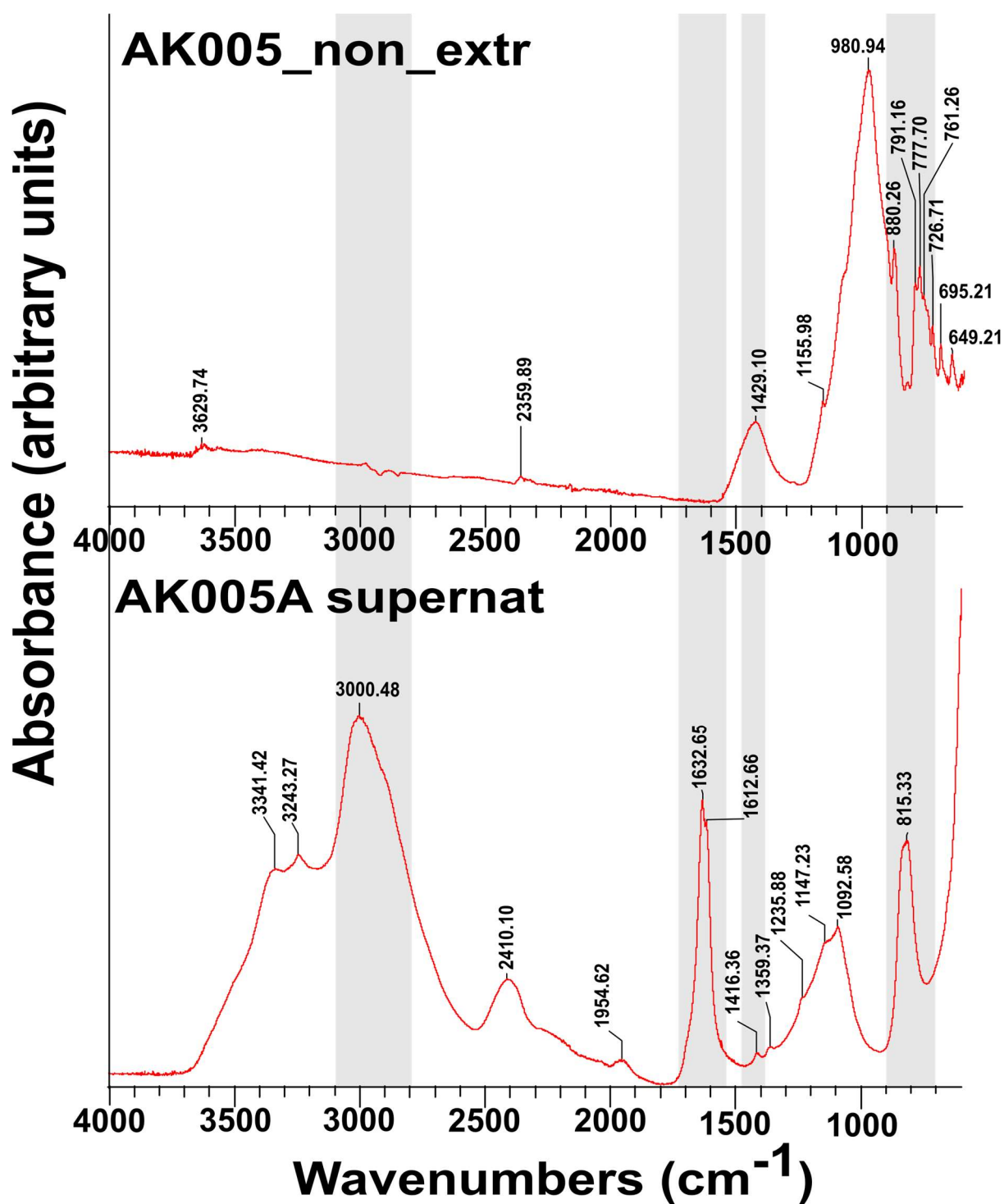
Figure 4.2.2. Comparison between IR spectra of a powdered dry sediment (top) and the extracted organic fraction. Absorption bands (highlighted in grey) include the C–H stretching region (3,100–3,000 cm^{-1}), the aliphatic C–H stretching region (3,000–2,800 cm^{-1}), the oxygenated groups and aromatic/olefinic region (1,550–1,750 cm^{-1}), and the aromatic out-of-plane C–H deformation region (700–900 cm^{-1}).

Shirin Baydjanova

As seen from Figure 4.2.2, after the removal of the overlapping carbonate matrix, the extracted supernatant shows a high thermal maturity of the sample. Unfortunately, the time constraints did not allow the author to process all six samples in the same manner.

Another analysis was made on the extraction III supernatant and compared to the FTIR analyses on thermal maturity by Lis et al. (2005) (Figure 4.2.3). FTIR data show that the peaks in the 2800-3000 cm^{-1} region become less pronounced with an increased thermal maturity, while peaks in the 1600 cm^{-1}, and 700 – 900 cm^{-1} regions are more pronounced in less thermally mature samples.

Vitrinite reflectance (R_0) is a key measure of OM thermal maturity. R_0 values of ≤ 0.5 indicate immature OM, R_0 values between 0.55%– 1.3% show that the OM is in the oil window, and R_0 values $\geq$ 1.3% indicate that the OM is over-mature and in the condensate/wet gas window (Peters et al., 2005). As can be seen from the Figure 4.2.3, both AK005 and Bao supernatants are well above R_0 1.4%.

Shirin Baydjanova
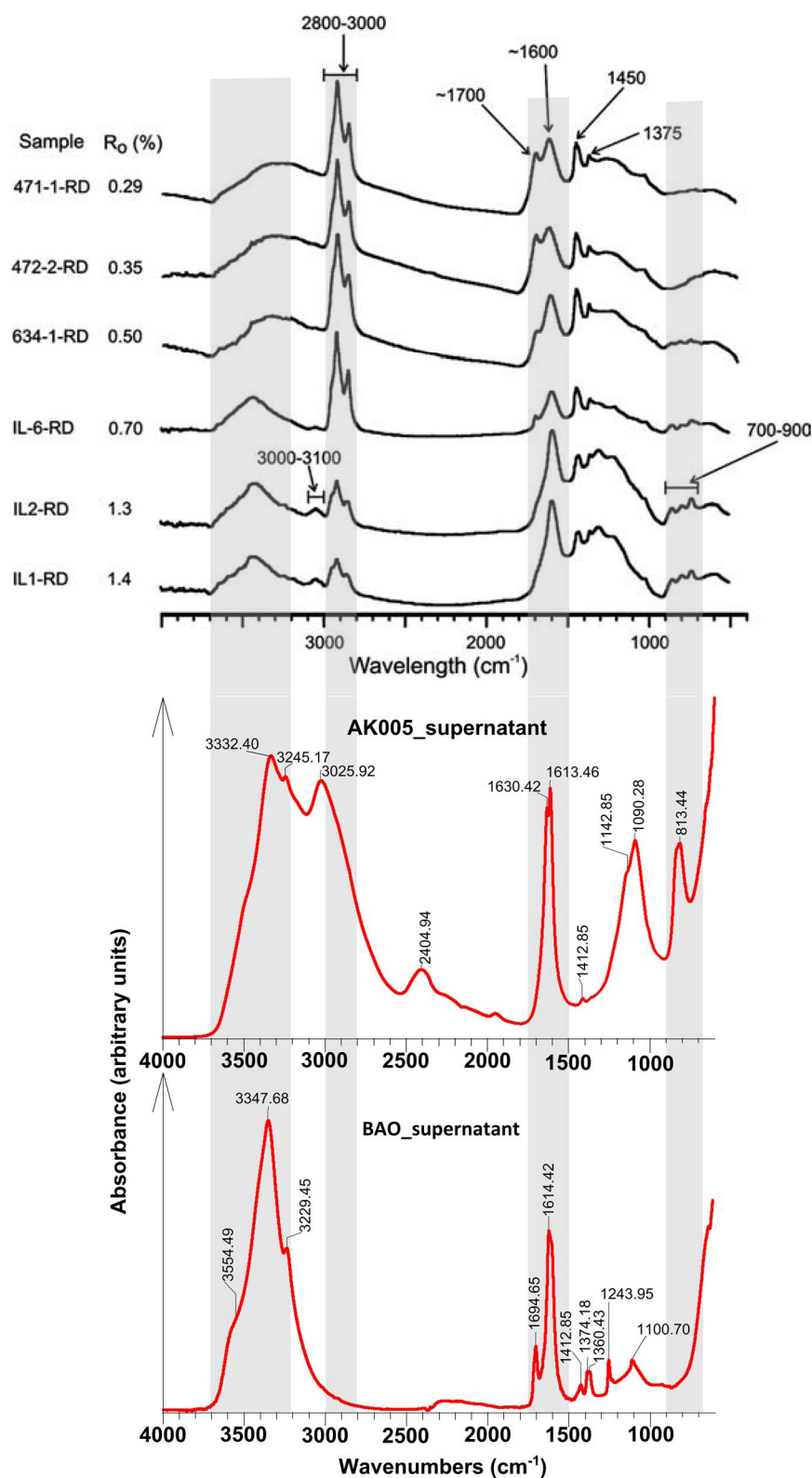
Figure 4.2.3. Comparison of Australian (AK005) and Namibian (BAO) supernatants with the FTIR on OM of different maturity (top). Note the vitrinite reflectance (R_0 %) values on the left increase downwards.

Shirin Baydjanova

There is a difference between these two samples in the 2800-3000 region. As shown in Figure 4.2.3, the peak in this region is present in the Australian AK005 sample and absent in the Namibian BAO sample. This could mean that the thermal maturity of the Namibian sample is slightly higher than of the Australian one.

4.3   Raman spectrometric analyses

Raman spectrometry was performed on samples AK019, AK005, BAO-2A, and Bull as well as on a graphite from the graphite mine in Ĉeskỷ Krumlov, Czech Republic. Raman spectrometry is able to differentiate between organic matter and graphitic carbons because of the difference in bandwidths (FWHM). Biogenic carbonaceous material usually displays wider bands as an indication of the degree of disorder. The "disordered" (D) OM peak occurs at $\sim$ 1350 cm^{-1} and the ordered graphite (G) peak occurs at $\sim$ 1600 cm^{-1} (Pasteris and Wopenka, 2003). An example of the changes in the peak widths and heights with progressive metamorphism was demonstrated by Pasteris and Wopenka (Figure 4.3.1).

Shirin Baydjanova
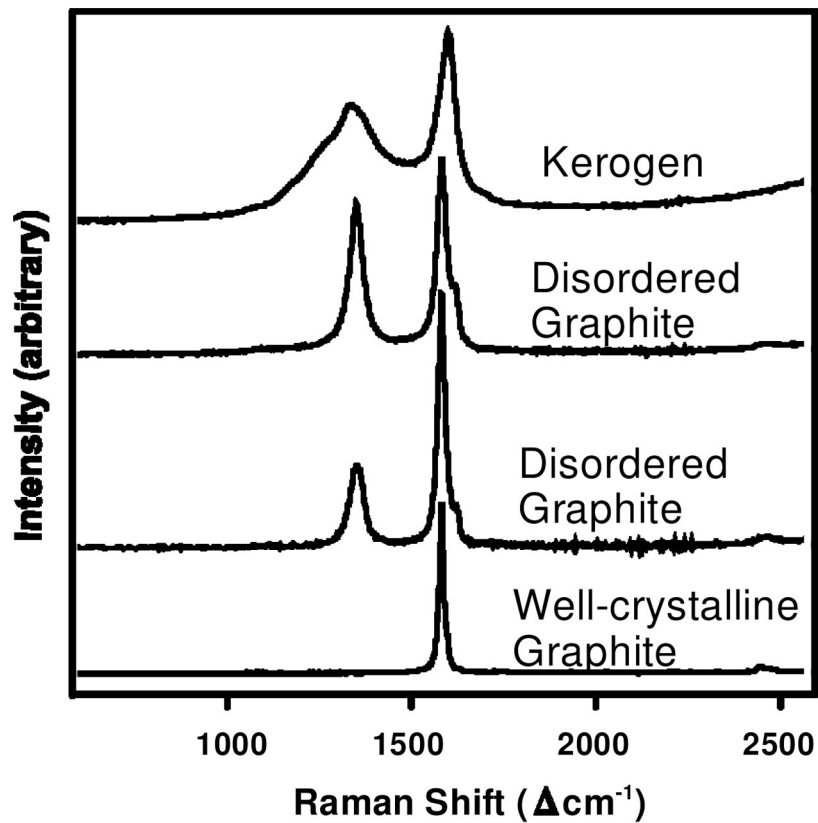
Figure 4.3.1. Comparison of the Raman spectra of carbonaceous samples showing progressive changes with increasing maturity. From top down: kerogen, low-grade metamorphism (chlorite zone), medium-grade metamorphism (garnet zone), and high-grade metamorphism (granulite facies) (Pasteris and Wopenka, 2003).

Representative comparison of the samples with un-metamorphosed kerogen and low-grade metamorphosed kerogen are given in Figure 4.3.2 and in Figure 4.3.3.

Shirin Baydjanova
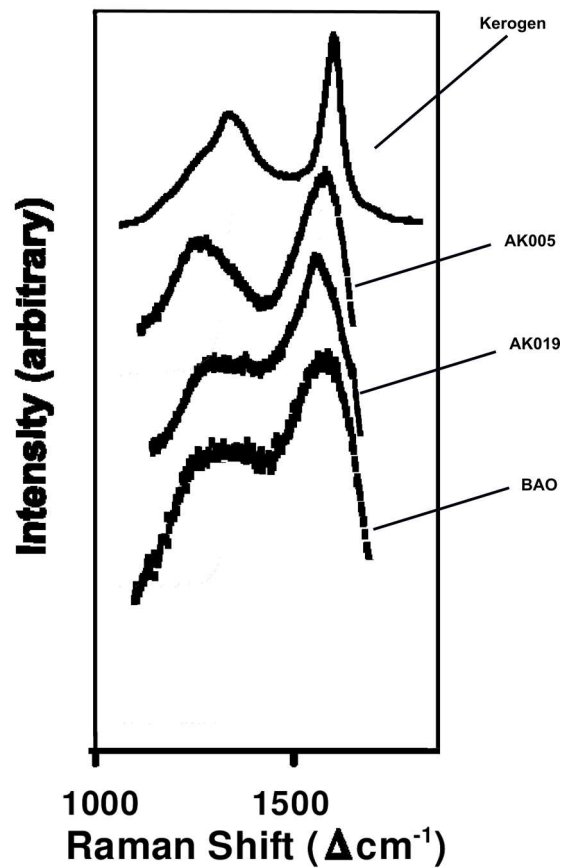
Figure 4.3.2. Comparison of the Raman spectra of measured samples with un-metamorphosed kerogen from Pasteris and Wopenka (2003) (top line).

Interestingly, the same samples exhibit a range of normal kerogen peaks and low-grade metamorphism peaks (Table 4.3.1). However, the wider range of D/G ratios is more common among Australian samples.

Shirin Baydjanova
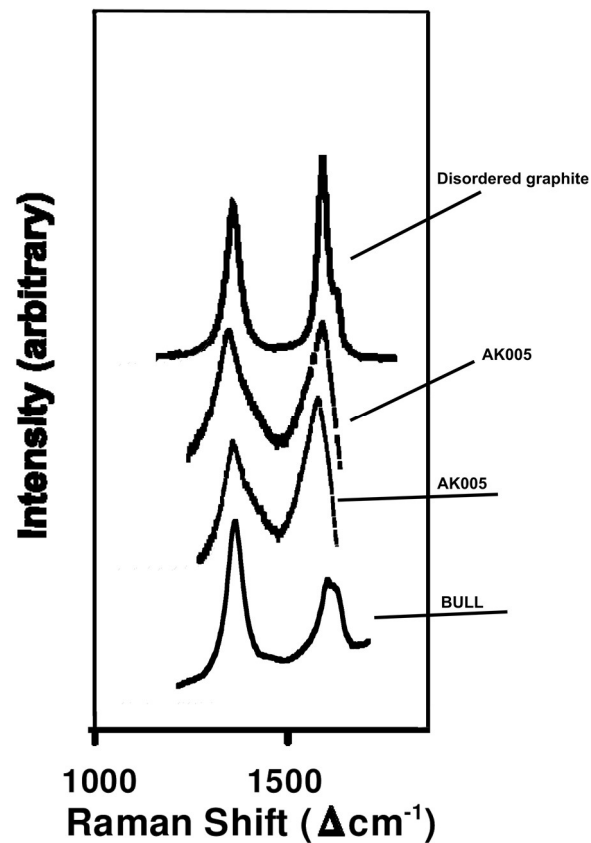
Figure 4.3.3. Comparison of the Raman spectra of measured samples with low-grade (chlorite zone) metamorphosed kerogen from Pasteris and Wopenka (2003) (top line).

Sample AK005 exhibits un-metamorphosed kerogen patterns and low-grade metamorphism patterns for different measurement points.

Comparison of the Ĉeský Krumlov graphite with the high-grade metamorphosed carbonaceous material from Pasteris and Wopenka (2003) can be seen in Figure 4.3.4.

Shirin Baydjanova
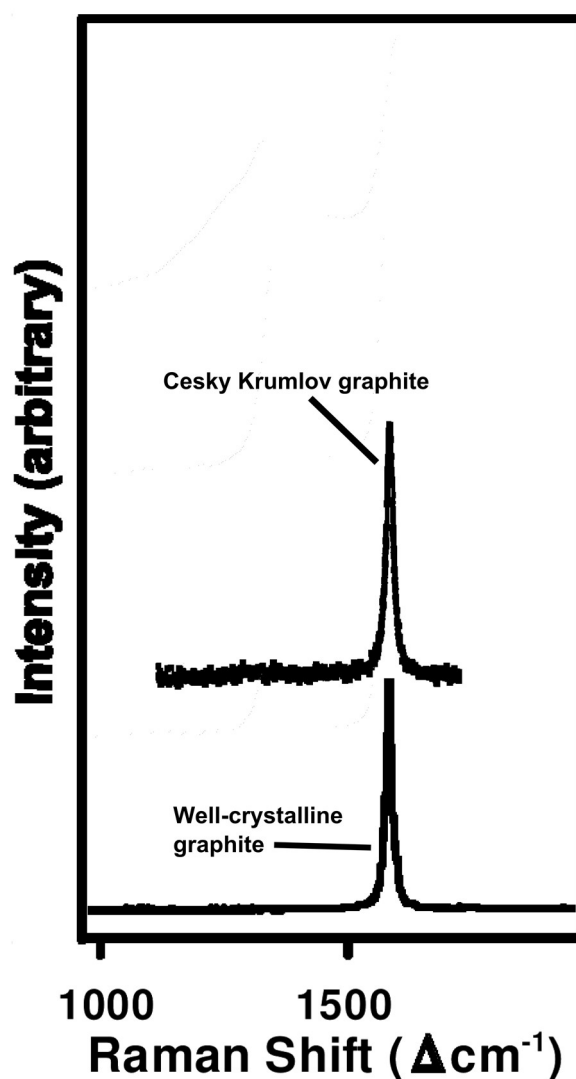
Figure 4.3.4. Comparison of the Raman spectra of measured graphite from the Ĉeský Krumlov graphite mine (top line) with high-grade metamorphosed kerogen (granulite facies) from Pasteris and Wopenka (2003).

Beyssac et al. (2002) stated that the lower the metamorphic grade, the larger is the ratio between the D and G peaks. With elevated metamorphism the ratio tends to become smaller. This could be explained by the changes in disordered (D) peak as the area of the peak becomes smaller due to the stiffening of aromatic planes. The ordered graphite peak, on the other hand, becomes more pronounced as more OM transforms to a more ordered state. Table 4.3.1 shows that samples AK005 and AK019 have high variability of ratios from very small (0.002) to very large (7.04) while sample BULL has quite small ratios of 0.6 and sample BAO has slightly larger ratios of ~ 1 and one ratio of 2.6. This shows that there is no homogeneity

Shirin Baydjanova

in metamorphic grades within Australian samples (AK005 and AK019). This is particularly obvious when the Raman data is combined with FTIR measurements on supernatants. As a supernatant is an extract of OM from the whole rock, it represents average thermal maturity values while Raman spectroscopy allows to look at different parts of the rock and different spots of OM.

Table 4.3.1. D/G ratio (by full width at half maximum (FWHM)).

Sample	D position	D FWHM	D intensity	G position	G FWHM	G intensity	D/G
Bull	1351.1	52.3	924.2	1592.9	85.9	529.2	0.6
	1366.7	52.3	346.8	1589.8	91.4	188.8	0.6
AK005	1351.3	118.7	1667.6	1552.4	125.6	2128.7	1.0
	1368.8	277.2	3767.8	1578.8	109.8	4150.9	2.5
	1344.9	395.6	2128.2	1529.1	135.3	1012.8	2.9
	1341.8	413.9	2545.1	1552.4	114.6	1287.3	3.6
	1349.7	266.4	3224.9	1578.8	113.8	2964.5	2.3
	1325.8	5.1	7906.0	1592.7	136.1	2977.3	0.04
	1360.8	333.9	5453.6	1570.0	127.1	5398.1	2.6
	1344.9	211.8	4484.3	1578.8	113.7	5602.5	1.9
	1348.1	247.2	2458.7	1578.8	123.3	2780.2	2.0
	1344.9	321.3	1815.2	1532.2	140.9	1374.7	2.3
	1356.1	253.0	2980.0	1574.1	112.4	3491.4	2.3
	13525.0	122.5	407.8	1585.2	141.4	903.4	0.9
	1344.9	205.8	3006.0	1578.8	130.6	2650.4	1.6
AK019	1324.4	474.5	3977.8	1573.3	213.5	2522.3	2.2
	1324.2	0.4	9413.2	1572.6	88.4	1614.3	0.004
	1324.3	6.7	4752.6	1574.2	62.6	1668.0	0.1
	1327.1	327.5	567.7	1580.1	123.9	577.5	2.6
	1325.7	448.0	1042.8	1583.5	183.7	667.3	2.4
	1326.6	6.3	825.5	1577.6	3003.5	46633.6	0.002
	1326.2	11.2	5818.2	1579.7	120.5	36989.4	0.09
	1327.5	6.5	471.9	1578.4	130.4	63.3	0.1
	1329.7	1337.5	10749.7	1588.2	190.0	795.4	7.04
	1330.6	117.7	731.2	1588.2	130.2	983.7	0.9
Bao-2A	1338.6	301.6	1041.4	1563.3	118.3	848.5	2.6
	1333.8	135.0	382.4	1569.5	138.9	1125.5	1.0
	1338.6	115.4	1084.6	1561.8	122.5	1640.8	0.9
	1321.0	120.9	354.8	1583.4	125.5	706.9	1.0
	1325.8	118.4	2623.8	1564.9	133.5	4769.9	0.9

Shirin Baydjanova

	1338.6	133.4	3363.4	1561.8	135.7	8501.6	1.0
	1319.4	62.0	7955.7	1569.5	62.9	5359.4	1.0

4.4 Molecular analyses

GC-MS analyses were carried out after every extraction method to check the type and amount of hydrocarbons extracted (all samples proved to be very lean with ~1–2 mg of dry EOM/g of rock powder). No hopanes or steranes were detected after each extraction, though, the amount of n-alkanes and some aromatic hydrocarbons increased with bitumen II extraction method, when 36% HCl was used to dissolve the rock powder (Figure 4.4.1). As the same powder was dissolved twice, the abundance of the hydrocarbons decreased considerably after the third extraction. However, the variability of the hydrocarbons increased.

Shirin Baydjanova
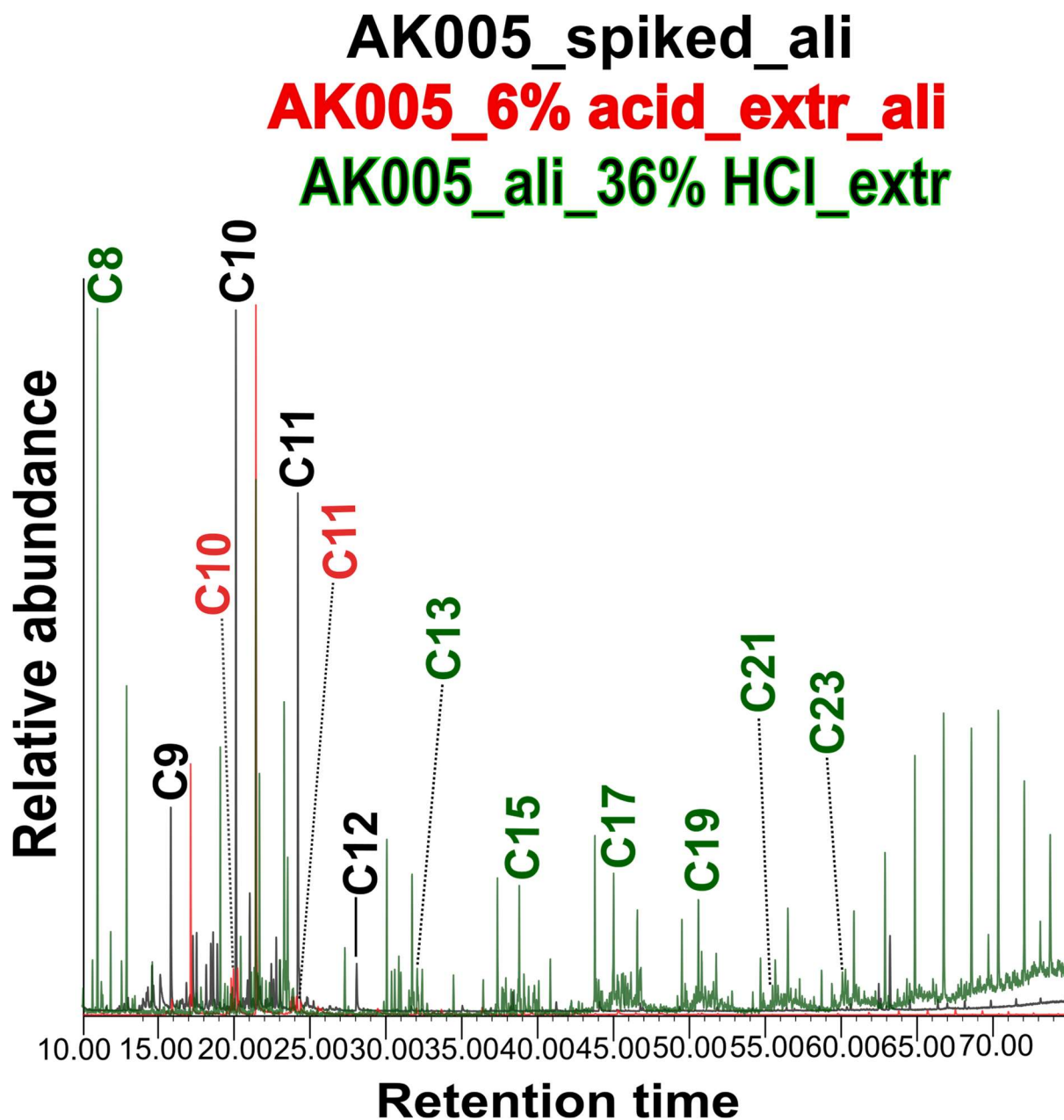
Figure 4.4.1. Partial m/z 57 mass chromatograms for samples AK005, showing comparison of the changes in hydrocarbons abundance and distribution between the three extraction methods. Black chromatogram – bitumen extraction I, red – bitumen extraction II with 6% HCl, green – bitumen extraction II with 36% HCl. Cx = # of n-alkane.

To exclude contamination, a basalt blank and a DCM blank were run at the same time (Figure 4.4.2; Figure 4.4.3).

Shirin Baydjanova
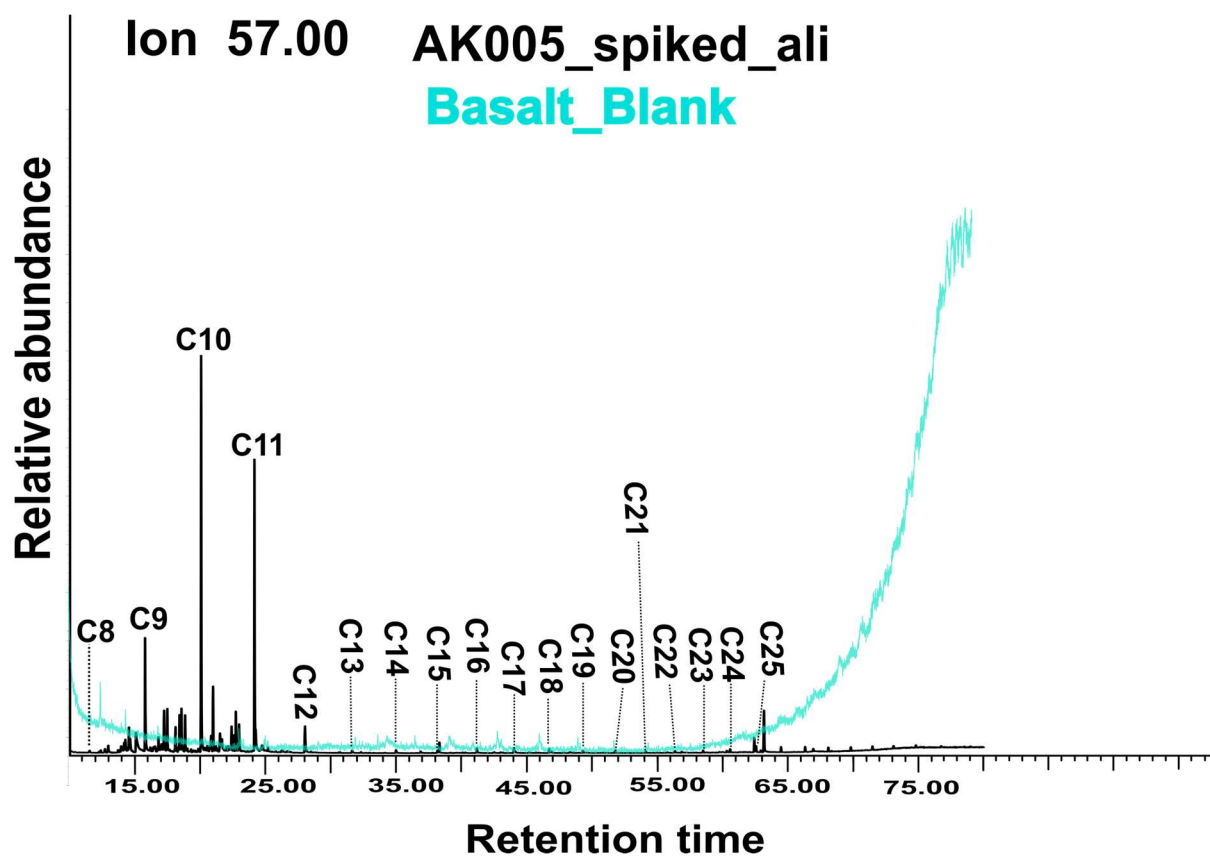
Figure 4.4.2. Partial m/z 57 chromatogram of sample AK005 (bitumen I extraction) and a basalt blank. Cx = # of n-alkane.
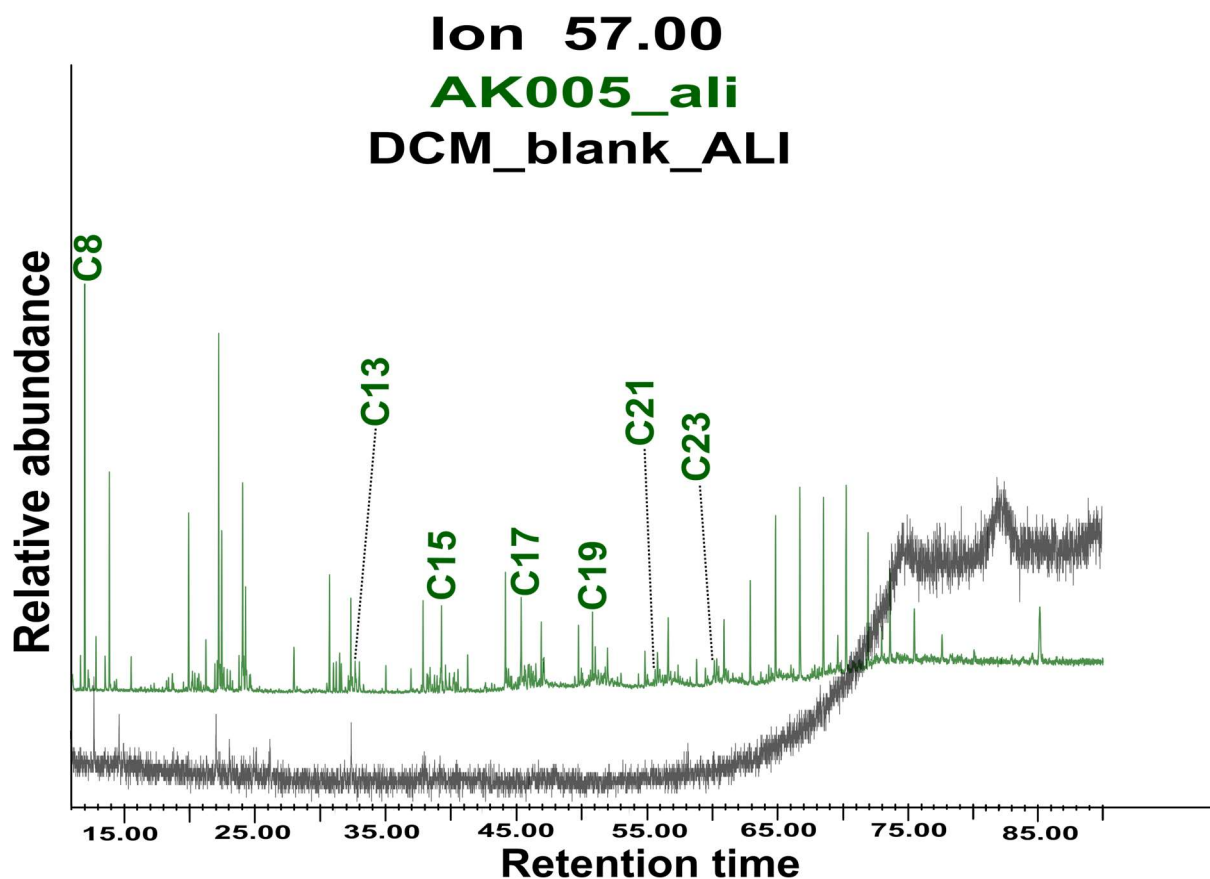
Figure 4.4.3. Partial m/z 57 chromatogram of sample AK005 (bitumen II extraction, 36% HCL) and a DCM blank. The chromatograms are deliberately offset for clearer view of the peaks. Cx = # of n-alkane.

Other hydrocarbons useful for the thermal maturity evaluation were low molecular weight (LMW) alkylbenzenes (Table 4.4.1). Thermal maturity and evaporative fractionation appear to be main controls of the distribution of LMW alkylbenzenes. With increased thermal maturity the concentrations of $C_0$-$C_2$ alkylbenzenes increases, so the ratio of C_{3-4}/C_{0-2} can be used as an indicator of thermal maturity (with the increase of C_0-C_2, the ratio becomes smaller) (Cheng et al., 2015). In this study, both benzene and toluene were not distinguishable from the solvent peak. As the result, the ratio was adjusted for use with the detected peaks.

Table 4.4.1. Ratios of low-molecular weight alkylbenzenes.

Sample	(C3+C4)/C2
AK017	1.0
AK005	3.1
AK019	2.4
HN2	2.5

Shirin Baydjanova

Bull	6.2
Bao-2A	1.9

According to the Table 4.4.1 the lowest ratios belong to the most thermally mature samples AK017 and Bao-2A while the least mature samples are AK005 and Bull.

Other useful maturity parameters are the ratios of naphthalene (N) and phenanthrene (P) to their methylated counterparts – methylnaphthalenes (MN), dimethylnaphthalenes (DMN), trimethylnaphthalenes (TMN), and methylphenanthrenes (MP) (Radke and Welte, 1981, van Aarssen et al., 1999, Peters et al., 2005). Methylnaphthalene has two isomers – 1-Methylnaphthalene (1MN, α isomer) and 2-Methylnaphthalene (2MN, β isomer). Methyphenanthrenes have two β isomers – 2MP and 3MP, which are more stable than two α isomers – 1MP and 9MP (Radke, 1987). These ratios tend to increase with increasing thermal maturity (Peters et al., 2005).

Table 4.4.2 shows the available ratios of these hydrocarbons. Not all ratios are available as only N and P are present in all samples. MP are sometimes present in AK017, BAO and Bull samples. Partial chromatograms of N, MP, and xylenes (C_2) are in Appendix C.

Table 4.4.2. Ratios of N to MN (N/Sum MN, MNR (2-/1-MN)) and dimethylnaphthalenes (DNR-x).

Sample name	N/ Sum MN	MNR (2-/1-MN)	DNR-x
AK005	0.7	1.7	n/a
AK017	0.2	1.9	n/a
AK019	5.2	1.7	n/a
BAO	5.5	2.3	n/a
BULL	17.5	2.8	1.1
HN2	12.7	2.2	n/a

Not all ratios from the table above correlate with each other. This can be explained by the fact that N, denominator in the first ratio, is more stable than the methylated naphthalenes. The same applies to the P and MP (van Aarssen et al., 1999). As was noted above, MP was not detected in all samples. In AK017, BAO, and Bull some peaks were present but in a very small amount and showed poor resolution. Thus, the MPI and MPR ratios could not be calculated.

Shirin Baydjanova

Chapter 5. Discussion

5.1 Biomarker findings

One of the main goals of this pilot study is to test the hypothesis that the chambered structures found in both suites of rocks (Wallace et al., 2014) are sponge fossils by using organic geochemistry techniques. Sponges are considered to be the first known animals, although the time of their appearance is still a controversial subject (Antcliffe, 2013). Finding biomarkers specific to sponges in the examined rocks could support the abovementioned hypothesis.

In order to verify this possibility, this study tried to find sterane biomarkers in the samples, in particular, C_{30} sterane. This biomarker has two isomers – 24-propylcholestane that is mostly produced by algae, and 24-isopropylcholestane that is a sponge biomarker (Love et al., 2009). However, no sterane biomarkers were discovered in the studied samples.

Interestingly, no hopane biomarkers were discovered either. Hopanes are biomarkers for prokaryotes, and finding them would suggest that the structures might have been of bacterial/microbial origin.

There are several possible explanations of the absence of these particular biomarkers, such as:

- the OM found in the rocks is of abiogenic origin
- the rocks are thermally over-mature and the biomarkers have been destroyed.

The theory of the abiogenic origin of some hydrocarbons has been widely discussed and there is an agreement that abiogenic formation mechanisms are a minor source of some hydrocarbons (Sherwood Lollar et al., 2002). It is possible to distinguish biogenic hydrocarbons from abiogenic ones by compound-specific isotope studies. This could be a future project, because compound-specific studies were unfortunately beyond the time constraints of this Masters project.

The option of over-maturation is also possible as during metagenesis the OM evolves into gases, such as methane, and carbon residue, and begins to develop some crystalline ordering (Tissot and Welte, 2012) with R_0 values less than 4% but more than 2% (Horsfield and Rullkotter, 1994). $R_0 > 4\%$ values correspond to the beginning of the greenschist facies (Tissot and Welte, 2012).

Shirin Baydjanova

The thermal maturity and the indigeneity of the biomarkers are two major problems that are present when studying the Precambrian rocks (Palacas, 1997, Brocks et al., 1999, Dutkiewicz et al., 2006, Brocks, 2011, French et al., 2015). The thermal maturity of the rocks in this study was tested widely using a combination of different techniques including Raman spectrometry, FTIR, SEM, and organic geochemistry. Despite the unfortunate outcome of this study, it should be noted that there are many Precambrian rocks that are not over mature and still contain indigenous biomarkers (Brocks et al., 2003, Love et al., 2009, Flannery and George, 2014, Jarrett, 2014, Hoshino et al., 2015). Apart from the organic rich, thermally mature Cryogenian rocks in Oman (Love et al., 2009), there are also organic rich rocks in the oil window in the Amadeus Basin, Australia (Jarrett, 2014), as been described in Chapter 2.

5.2   Thermal maturity

The SEM examinations have revealed that only the Australian samples (AK005, AK017, and AK019) contain discrete OM, which is not included in the carbonate minerals. The Namibian samples (Bao-2A, Bull, and Huab North 2), on the other hand, contain only OM included within the calcite and dolomite grains. The latter can be due to a higher degree of metamorphism, which could have led to loss of any discrete OM, while any OM protected by the carbonate hosts was unaffected. During early diagenesis organic carbon particles could be "captured" by precipitating carbonates, thus removing the OM from circulation and protecting them from the temperature changes. It is possible that the "free" OM had been obliterated by high temperatures, especially if some catalysts such as clay or iron sulphides were present (Peters et al., 2005, Cheng et al., 2015). We know that haematite was definitely present at least in the Namibian samples (Hoffman, 2002). Small particles of iron oxides were also seen by the petrographic examination of the Australian samples.

The FTIR analysis on extracted supernatants and comparisons with other supernatants of known maturity showed that both samples (AK005 and Bao-2A) are in the over-mature window. Considering the bulk nature of the FTIR results, the samples still can contain OM spots of lower maturity.

Raman spectrometry investigated approximately 2 μm analysis spots; this can help assess the thermal maturity of individual spots of OM. This analysis has shown more homogeneity in thermal maturity within the Namibian samples. In contrast, the Australian samples show both high and low thermal maturity results, which suggest thermal heterogeneity within the

Shirin Baydjanova

samples. None of the samples show graphite peaks. That must mean that the samples did not undergo high-grade metamorphism (either garnet zone or granulite facies). However, the Namibian samples mostly have peaks in the low-grade (chlorite zone) metamorphism and only a few un-metamorphosed kerogen peaks, while the Australian samples show kerogen peaks as well as the peaks corresponding to low-grade metamorphism (Figure 4.3.2; Figure 4.3.3).

This may indicate that the Australian samples are of lower thermal maturity compared to the Namibian samples and still have a potential to yield some biomarkers if the HydroPyrolysis (HyPy) technique was applied (Love et al., 1995, Wu et al., 2015). Unfortunately, the organic geochemistry lab in Macquarie University does not have this equipment, however, it may be possible to apply HyPy in a future study.

GC-MS data correlate with the FTIR and Raman data and indicate a high thermal maturity of the organic matter in both sets of samples. Apparently, the samples were subjected to a high enough temperature that all hopane and sterane biomarkers were obliterated, if these originally existed. The presence of LMW alkylbenzenes also indicates high thermal maturity because during very high thermal maturation more LMW hydrocarbons are produced during cracking, and these are more thermally resistant (Peters et al., 2005).

Sadly, this study could not confirm or disprove whether the structured chambers in both sets of samples could belong to the proto-sponges. Due to the absence of hopanes it is not even possible to suggest if the chambered structures could be produced by microbial biota. Nevertheless, the negative results should not discourage scientists from other attempts to shed some light on the appearance and evolution of animals.

There are more samples available from the northern Flinders Ranges as more than 30 of them were collected. Other Namibian samples (Gobabis Formation) from the Kalahari Craton are also available. The Kalahari Craton has very different thermal history and reported to be organically rich (TOC~ 3%) (M.Kennedy, 2015, personal communication). However, this was a short pilot investigation and not all samples could be studied in the timeframe of 9 months. Further and longer type of study like a PhD project could be more fruitful.

Shirin Baydjanova

Chapter 6. Conclusions

The combination of SEM, Raman, FTIR, and GC-MS techniques all point to the organic matter in the studied samples being in the over-thermally mature window, above R_0 1.4%. The results show that overall the Namibian samples Bao-2A, Bull, and Huab North 2 are more mature than the Australian samples AK005, AK017, and AK019.

From the biomarker analysis point of view these results cannot confirm whether the chambered structures in the samples represent sponge fossils. Further biomarker studies of early sponges will need to focus on finding samples of the same age and of lower thermal maturity. The heterogeneity in thermal maturity in the Australian samples may suggest that some localities in the Northern Flinders Ranges potentially have rocks of lower thermal maturity, which would thus be more suitable for future biomarker studies. Raman and FTIR spectroscopy can help determine the feasibility of the biomarker analysis of the samples.

Furthermore, compound-specific isotopic studies of hydrocarbons can be suggested in the further research to exclude an abiogenic origin of the OM in the samples.

References

ANTCLIFFE, J. B. 2013. Questioning the Evidence of Organic Compounds Called Sponge Biomarkers. *Palaeontology,* 56**,** 917-925.

BEYSSAC, O., GOFFÉ, B., CHOPIN, C. & ROUZAUD, J. 2002. Raman Spectra of Carbonaceous Material in Metasediments: A New Geothermometer. *Journal of metamorphic Geology,* 20**,** 859-871.

BONS, P. D., MONTENARI, M., BAKKER, R. J. & ELBURG, M. A. 2009. Potential Evidence of Fossilised Neoproterozoic Deep Life: Sem Observations on Calcite Veins from Oppaminda Creek, Arkaroola, South Australia. *International Journal of Earth Sciences,* 98**,** 327-343.

BOSAK, T., LAHR, D., PRUSS, S., MACDONALD, F., DALTON, L. & MATYS, E. 2011. Agglutinated Tests in Post-Sturtian Cap Carbonates of Namibia and Mongolia. *Earth and Planetary Science Letters,* 308**,** 29-40.

BRAIN, C. B., PRAVE, A. R., HOFFMANN, K.-H., FALLICK, A. E., BOTHA, A., HERD, D. A., STURROCK, C., YOUNG, I., CONDON, D. J. & ALLISON, S. G. 2012. The First Animals: Ca. 760-Million-Year-Old Sponge-Like Fossils from Namibia. *South African Journal of Science,* 108**,** 01-08.

BROCKS, J. J. 2011. Millimeter-Scale Concentration Gradients of Hydrocarbons in Archean Shales: Live-Oil Escape or Fingerprint of Contamination? *Geochimica et Cosmochimica Acta,* 75**,** 3196-3213.

BROCKS, J. J., BUICK, R., LOGAN, G. A. & SUMMONS, R. E. 2003. Composition and Syngeneity of Molecular Fossils from the 2.78 to 2.45 Billion-Year-Old Mount Bruce Supergroup, Pilbara Craton, Western Australia. *Geochimica et Cosmochimica Acta,* 67**,** 4289-4319.

Shirin Baydjanova

BROCKS, J. J., LOGAN, G. A., BUICK, R. & SUMMONS, R. E. 1999. Archean Molecular Fossils and the Early Rise of Eukaryotes. *Science,* 285**,** 1033-1036.

BUTTERFIELD, N. J. 2000. Bangiomorpha Pubescens N. Gen., N. Sp.: Implications for the Evolution of Sex, Multicellularity, and the Mesoproterozoic/Neoproterozoic Radiation of Eukaryotes. *Journal Information,* 26.

CANFIELD, D. E. 2005. The Early History of Atmospheric Oxygen: Homage to Robert M. Garrels. *Annual Review of Earth and Planetary Sciences,* 33**,** 1-36.

CHENG, B., WANG, T., HUANG, H., WANG, G. & SIMONEIT, B. R. T. 2015. Ratios of Low Molecular Weight Alkylbenzenes (C0–C4) in Chinese Crude Oils as Indicators of Maturity and Depositional Environment. *Organic Geochemistry,* 88**,** 78-90.

CORSETTI, F. A., AWRAMIK, S. M. & PIERCE, D. 2003. A Complex Microbiota from Snowball Earth Times: Microfossils from the Neoproterozoic Kingston Peak Formation, Death Valley, USA. *Proceedings of the National Academy of Sciences,* 100**,** 4399-4404.

DEER, W. A., HOWIE, R. A. & ZUSSMAN, J. 1992. *An Introduction to the Rock-Forming Minerals*, Longman London.

DOOLITTLE, R. F., FENG, D.-F., TSANG, S., CHO, G. & LITTLE, E. 1996. Determining Divergence Times of the Major Kingdoms of Living Organisms with a Protein Clock. *Science,* 271**,** 470-477.

DUTKIEWICZ, A., VOLK, H., GEORGE, S. C., RIDLEY, J. & BUICK, R. 2006. Biomarkers from Huronian Oil-Bearing Fluid Inclusions: An Uncontaminated Record of Life before the Great Oxidation Event. *Geology,* 34**,** 437-440.

DUTKIEWICZ, A., VOLK, H., RIDLEY, J. & GEORGE, S. 2004. Geochemistry of Oil in Fluid Inclusions in a Middle Proterozoic Igneous Intrusion: Implications for the Source of Hydrocarbons in Crystalline Rocks. *Organic Geochemistry,* 35**,** 937-957.

FARQUHAR, J. & WING, B. A. 2003. Multiple Sulfur Isotopes and the Evolution of the Atmosphere. *Earth and Planetary Science Letters,* 213**,** 1-13.

FLANNERY, E. N. & GEORGE, S. C. 2014. Assessing the Syngeneity and Indigeneity of Hydrocarbons in the~ 1.4 Ga Velkerri Formation, Mcarthur Basin, Using Slice Experiments. *Organic Geochemistry,* 77**,** 115-125.

FRENCH, K. L., HALLMANN, C., HOPE, J. M., SCHOON, P. L., ZUMBERGE, J. A., HOSHINO, Y., PETERS, C. A., GEORGE, S. C., LOVE, G. D. & BROCKS, J. J. 2015. Reappraisal of Hydrocarbon Biomarkers in Archean Rocks. *Proceedings of the National Academy of Sciences,* 112**,** 5915-5920.

FROMHOLD, T. & WALLACE, M. 2011. Nature and Significance of the Neoproterozoic Sturtian–Marinoan Boundary, Northern Adelaide Geosyncline, South Australia. *Australian Journal of Earth Sciences,* 58**,** 599-613.

GIDDINGS, J., WALLACE, M. & WOON, E. 2009. Interglacial Carbonates of the Cryogenian Umberatana Group, Northern Flinders Ranges, South Australia. *Australian Journal of Earth Sciences,* 56**,** 907-925.

GRAZHDANKIN, D. 2004. Patterns of Distribution in the Ediacaran Biotas: Facies Versus Biogeography and Evolution. *Paleobiology,* 30**,** 203-221.

GUNASEKARAN, S., ANBALAGAN, G. & PANDI, S. 2006. Raman and Infrared Spectra of Carbonates of Calcite Structure. *Journal of Raman Spectroscopy,* 37**,** 892-899.

HOERING, T. 1965. The Extractable Organic Matter in Precambrian Rocks and the Problem of Contamination. *Carnegie Institution of Washington Yearbook,* 64**,** 215-218.

HOFFMAN, P. Carbonates Bounding Glacial Deposits: Evidence for Snowball Earth Episodes and Greenhouse Aftermaths in the Neoproterozoic Otavi Group of Northern

Shirin Baydjanova

Namibia. Excursion Guide, 16th Int. Sedimentological Conf.(International Association of Sedimentologists, 2002), 2002.

HOFFMAN, P., HAWKINS, D., ISACHSEN, C. & BOWRING, S. 1996. Precise U–Pb Zircon Ages for Early Damaran Magmatism in the Summas Mountains and Welwitschia Inlier, Northern Damara Belt, Namibia. *Communications of the geological survey of Namibia,* 11**,** 47-52.

HOFFMANN, K. New Constraints on the Timing of Continental Breakup and Collision in the Damara Belt. Proterozoic Crustal and Metallogenic Evolution. Abstracts of Geological Society and Geological Survey of Namibia Conference, Windhoek, 1994. 30.

HOFFMANN, K. & PRAVE, A. 1996. A Preliminary Note on a Revised Subdivision and Regional Correlation of the Otavi Group Based on Glaciogenic Diamictites and Associated Cap Dolostones. *Communications of the geological survey of Namibia,* 11**,** 77-82.

HOFMANN, H., NARBONNE, G. & AITKEN, J. 1990. Ediacaran Remains from Intertillite Beds in Northwestern Canada. *Geology,* 18**,** 1199-1202.

HOLLAND, H. D. 2006. The Oxygenation of the Atmosphere and Oceans. *Philosophical Transactions of the Royal Society of London B: Biological Sciences,* 361**,** 903-915.

HOOD, A., WALLACE, M. W. & DRYSDALE, R. N. 2011. Neoproterozoic Aragonite-Dolomite Seas? Widespread Marine Dolomite Precipitation in Cryogenian Reef Complexes. *Geology,* 39**,** 871-874.

HORSFIELD, B. & RULLKOTTER, J. 1994. Diagenesis, Catagenesis, and Metagenesis of Organic Matter: Chapter 10: Part Iii. Processes.

HOSHINO, Y. 2015. *Investigation of Hydrocarbon Biomarkers Preserved in the Fortescue Group in the Pilbara Craton, Western Australia* PhD, Macquarie University.

HOSHINO, Y., FLANNERY, D., WALTER, M. & GEORGE, S. 2015. Hydrocarbons Preserved in a~ 2.7 Ga Outcrop Sample from the Fortescue Group, Pilbara Craton, Western Australia. *Geobiology,* 13**,** 99-111.

HOSHINO, Y. & GEORGE, S. C. 2015. Cyanobacterial Inhabitation on Archean Rock Surfaces in the Pilbara Craton, Western Australia. *Astrobiology,* 15**,** 559-574.

ILLING, C. J., HALLMANN, C., MILLER, K. E., SUMMONS, R. E. & STRAUSS, H. 2014. Airborne Hydrocarbon Contamination from Laboratory Atmospheres. *Organic Geochemistry,* 76**,** 26-38.

JARRETT, A. 2014. A Neoproterozoic Environmental Reconstruction of the Amadeus Basin, Central Australia Using Biomarkers and Redox Chemistry. *ANU,* PhD thesis.

JI, J., GE, Y., BALSAM, W., DAMUTH, J. E. & CHEN, J. 2009. Rapid Identification of Dolomite Using a Fourier Transform Infrared Spectrophotometer (Ftir): A Fast Method for Identifying Heinrich Events in Iodp Site U1308. *Marine Geology,* 258**,** 60-68.

JOHNSTON, D. T., WOLFE-SIMON, F., PEARSON, A. & KNOLL, A. H. 2009. Anoxygenic Photosynthesis Modulated Proterozoic Oxygen and Sustained Earth's Middle Age. *Proceedings of the National Academy of Sciences,* 106**,** 16925-16929.

KAUFMAN, A. J., HAYES, J., KNOLL, A. H. & GERMS, G. J. 1991. Isotopic Compositions of Carbonates and Organic Carbon from Upper Proterozoic Successions in Namibia: Stratigraphic Variation and the Effects of Diagenesis and Metamorphism. *Precambrian Research,* 49**,** 301-327.

KELLY, A. E., LOVE, G. D., ZUMBERGE, J. E. & SUMMONS, R. E. 2011. Hydrocarbon Biomarkers of Neoproterozoic to Lower Cambrian Oils from Eastern Siberia. *Organic Geochemistry,* 42**,** 640-654.

Shirin Baydjanova

KNOLL, A. H. 1992. The Early Evolution of Eukaryotes: A Geological Perspective. *Science,* 256**,** 622-627.

KNOLL, A. H. 1999. Early Animal Evolution: Emerging Views from Comparative Biology and Geology. *Science,* 284**,** 2129-2137.

KNOLL, A. H. 2003. *Life on a Young Planet: The First Three Billion Years of Evolution on Earth*, Princeton University Press.

KNOLL, A. H. 2014. Paleobiological Perspectives on Early Eukaryotic Evolution. *Cold Spring Harb Perspect Biol,* 6.

KROENER, A. 1982. Rb-Sr Geochronology and Tectonic Evolution of the Pan-African Damara Belt of Namibia, Southwestern Africa. *Am. J. Sci,* 282**,** 1471-1507.

LAFLAMME, M. 2010. Palaeontology: Wringing out the Oldest Sponges. *Nature Geoscience,* 3**,** 597-598.

LE BER, E., LE HERON, D. P., WINTERLEITNER, G., BOSENCE, D. W., VINING, B. A. & KAMONA, F. 2013. Microbialite Recovery in the Aftermath of the Sturtian Glaciation: Insights from the Rasthof Formation, Namibia. *Sedimentary Geology,* 294**,** 1-12.

LIS, G. P., MASTALERZ, M., SCHIMMELMANN, A., LEWAN, M. D. & STANKIEWICZ, B. A. 2005. Ftir Absorption Indices for Thermal Maturity in Comparison with Vitrinite Reflectance R 0 in Type-Ii Kerogens from Devonian Black Shales. *Organic Geochemistry,* 36**,** 1533-1552.

LOVE, G. D., GROSJEAN, E., STALVIES, C., FIKE, D. A., GROTZINGER, J. P., BRADLEY, A. S., KELLY, A. E., BHATIA, M., MEREDITH, W. & SNAPE, C. E. 2009. Fossil Steroids Record the Appearance of Demospongiae During the Cryogenian Period. *Nature,* 457**,** 718-721.

LOVE, G. D., SNAPE, C. E., CARR, A. D. & HOUGHTON, R. C. 1995. Release of Covalently-Bound Alkane Biomarkers in High Yields from Kerogen Via Catalytic Hydropyrolysis. *Organic Geochemistry,* 23**,** 981-986.

MALOOF, A. C., ROSE, C. V., BEACH, R., SAMUELS, B. M., CALMET, C. C., ERWIN, D. H., POIRIER, G. R., YAO, N. & SIMONS, F. J. 2010. Possible Animal-Body Fossils in Pre-Marinoan Limestones from South Australia. *Nature Geoscience,* 3**,** 653-659.

MASTANDREA, A., GUIDO, A., DEMASI, F., RUFFOLO, S. A. & RUSSO, F. 2011. The Characterisation of Sedimentary Organic Matter in Carbonates with Fourier-Transform Infrared (Ftir) Spectroscopy. *Advances in Stromatolite Geobiology.* Springer.

MCCALL, G. J. H. 2006. The Vendian (Ediacaran) in the Geological Record: Enigmas in Geology's Prelude to the Cambrian Explosion. *Earth-Science Reviews,* 77**,** 1-229.

MCKIRDY, D., SUMARTOJO, J., TUCKER, D. & GOSTIN, V. 1975. Organic, Mineralogic and Magnetic Indications of Metamorphism in the Tapley Hill Formation, Adelaide Geosyncline. *Precambrian Research,* 2**,** 345-373.

MCKIRDY, D. M., BURGESS, J. M., LEMON, N. M., YU, X., COOPER, A. M., GOSTIN, V. A., JENKINS, R. J. & BOTH, R. A. 2001. A Chemostratigraphic Overview of the Late Cryogenian Interglacial Sequence in the Adelaide Fold-Thrust Belt, South Australia. *Precambrian Research,* 106**,** 149-186.

MEERT, J. G., GIBSHER, A. S., LEVASHOVA, N. M., GRICE, W. C., KAMENOV, G. D. & RYABININ, A. B. 2011. Glaciation and ~770ma Ediacara (?) Fossils from the Lesser Karatau Microcontinent, Kazakhstan. *Gondwana Research,* 19**,** 867-880.

MOCZYDŁOWSKA, M. 2008. The Ediacaran Microbiota and the Survival of Snowball Earth Conditions. *Precambrian Research,* 167**,** 1-15.

Shirin Baydjanova

MUNSON, T. J. 2014. Petroleum Geology and Potential of the Onshore Northern Territory. *Northern Territory Geological Survey,* Report 22.

NABBEFELD, B., GRICE, K., SCHIMMELMANN, A., SUMMONS, R. E., TROITZSCH, U. & TWITCHETT, R. J. 2010. A Comparison of Thermal Maturity Parameters between Freely Extracted Hydrocarbons (Bitumen I) and a Second Extract (Bitumen Ii) from within the Kerogen Matrix of Permian and Triassic Sedimentary Rocks. *Organic Geochemistry,* 41**,** 78-87.

NARBONNE, G. 2008. *The Gaskiers Glaciation as a Significant Divide in Ediacaran History and Stratigraphy* [Online]. Available: http://www.cprm.gov.br/33IGC/1342961.html [Accessed 20th September 2014].

NARBONNE, G., XIAO, S., SHIELDS, G., GRADSTEIN, F., OGG, J., SCHMITZ, M. & OGG, G. 2012. The Ediacaran Period. *Geologic Timescale***,** 427-449.

OEHLER, J. H. 1977. Irreversible Contamination of Precambrian Kerogen by 14 C-Labelled Organic Compounds. *Precambrian Research,* 4**,** 221-227.

PALACAS, J. G. 1997. Source Rock Potential of Precambrian Rocks in Selected Basins of the United States. *US Geological Survey Bulletin,* 2146**,** 127-134.

PASTERIS, J. D. & WOPENKA, B. 2003. Necessary, but Not Sufficient: Raman Identification of Disordered Carbon as a Signature of Ancient Life. *Astrobiology,* 3**,** 727-738.

PAUL, E., FLÖTTMANN, T. & SANDIFORD, M. 1999. Structural Geometry and Controls on Basement‐Involved Deformation in the Northern Flinders Ranges, Adelaide Fold Belt, South Australia. *Australian Journal of Earth Sciences,* 46**,** 343-354.

PETERS, K., WALTERS, C. & MOLDOWAN, J. 2005. The Biomarker Guide, Biomarkers and Isotopes in Petroleum Exploration and Earth History, Vol 1–2. Cambridge University Press New York.

PETERSON, K. J., MCPEEK, M. A. & EVANS, D. A. 2005. Tempo and Mode of Early Animal Evolution: Inferences from Rocks, Hox, and Molecular Clocks. *Paleobiology,* 31**,** 36-55.

PIERREHUMBERT, R. T., ABBOT, D. S., VOIGT, A. & KOLL, D. 2011. Climate of the Neoproterozoic. *Annual Review of Earth and Planetary Sciences,* 39**,** 417-460.

PRUSS, S. B., BOSAK, T., MACDONALD, F. A., MCLANE, M. & HOFFMAN, P. F. 2010. Microbial Facies in a Sturtian Cap Carbonate, the Rasthof Formation, Otavi Group, Northern Namibia. *Precambrian Research,* 181**,** 187-198.

RADKE, M. 1987. Organic Geochemistry of Aromatic Hydrocarbons. *Advances in petroleum geochemistry,* 2**,** 141-207.

RADKE, M. & WELTE, D. 1981. The Methylphenanthrene Index (Mpi): A Maturity Parameter Based on Aromatic Hydrocarbons. *Advances in organic geochemistry,* 1983**,** 504-512.

REIG, F. B., ADELANTADO, J. G. & MORENO, M. M. 2002. Ftir Quantitative Analysis of Calcium Carbonate (Calcite) and Silica (Quartz) Mixtures Using the Constant Ratio Method. Application to Geological Samples. *Talanta,* 58**,** 811-821.

SHERWOOD LOLLAR, B., WESTGATE, T., WARD, J., SLATER, G. & LACRAMPE-COULOUME, G. 2002. Abiogenic Formation of Alkanes in the Earth's Crust as a Minor Source for Global Hydrocarbon Reservoirs. *Nature,* 416**,** 522-524.

TISSOT, B. & WELTE, D. 2012. *Petroleum Formation and Occurrence: A New Approach to Oil and Gas Exploration*, Springer Science & Business Media.

VAN AARSSEN, B. G., BASTOW, T. P., ALEXANDER, R. & KAGI, R. I. 1999. Distributions of Methylated Naphthalenes in Crude Oils: Indicators of Maturity, Biodegradation and Mixing. *Organic Geochemistry,* 30**,** 1213-1227.

Shirin Baydjanova

WALLACE, M. W., HOOD, A., WOON, E. M., HOFFMANN, K.-H. & REED, C. P. 2014. Enigmatic Chambered Structures in Cryogenian Reefs: The Oldest Sponge-Grade Organisms? *Precambrian Research,* 255**,** 109-123.

WANG, D. Y.-C., KUMAR, S. & HEDGES, S. B. 1999. Divergence Time Estimates for the Early History of Animal Phyla and the Origin of Plants, Animals and Fungi. *Proceedings of the Royal Society of London. Series B: Biological sciences,* 266**,** 163-171.

WRAY, G. A., LEVINTON, J. S. & SHAPIRO, L. H. 1996. Molecular Evidence for Deep Precambrian Divergences among Metazoan Phyla. *Science,* 274**,** 568-573.

WU, L., LIAO, Y. & GENG, A. 2015. Investigation of Hydropyrolysis Released Aromatic Hydrocarbons from Permian Kerogens at Different Maturities in the Sichuan Basin, China. *Journal of Analytical and Applied Pyrolysis,* 114**,** 47-59.

XIAO, S. 2004. Neoproterozoic Glaciations and the Fossil Record. *The Extreme Proterozoic: Geology, Geochemistry, and Climate***,** 199-214.

YIN, Z., ZHU, M., DAVIDSON, E. H., BOTTJER, D. J., ZHAO, F. & TAFFOREAU, P. 2015. Sponge Grade Body Fossil with Cellular Resolution Dating 60 Myr before the Cambrian. *Proceedings of the National Academy of Sciences,* 112**,** E1453-E1460.

Shirin Baydjanova

Appendix A. FTIR figures from methods chapter.
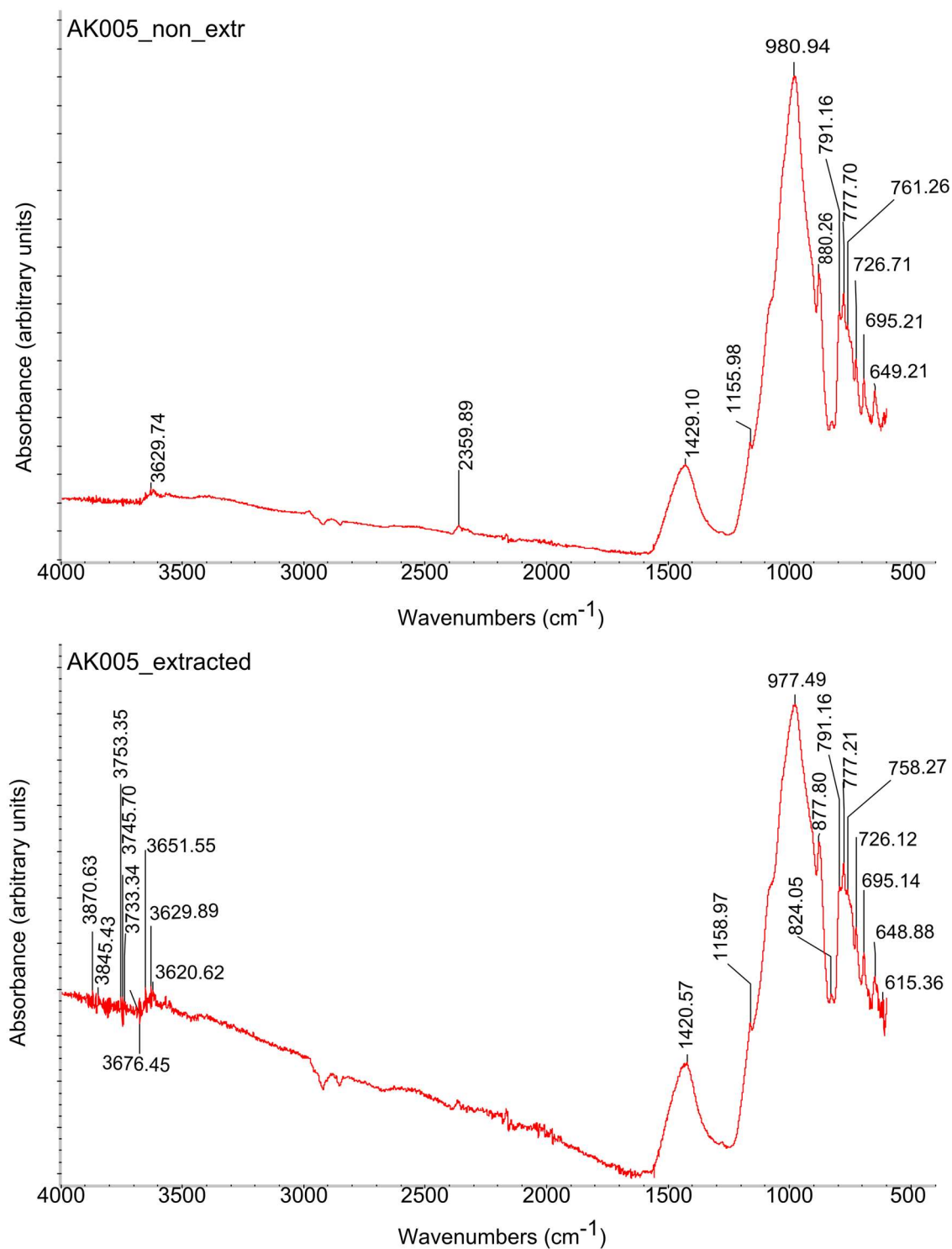
Figure A.1. Comparison of FTIR spectra of non-extracted rock powder and a residue of extraction I. Note the strong similarity between the two spectra.

Shirin Baydjanova
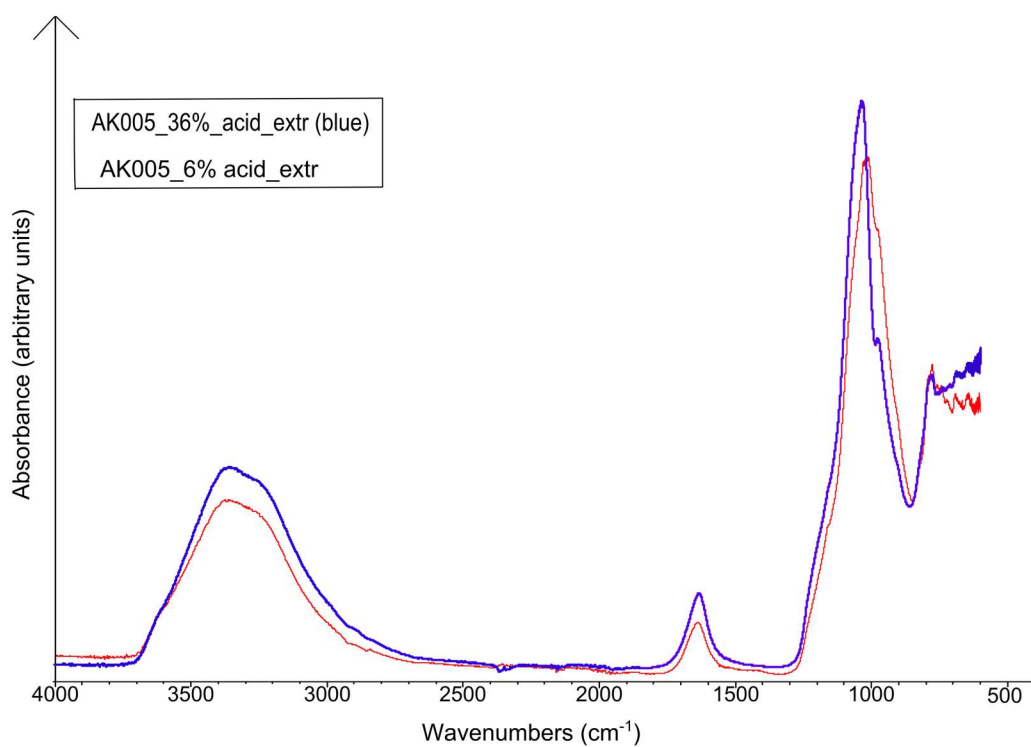
Figure A.2. FTIR spectra comparison of the residue after 6% HCl dissolution (red line) and 36% HCl dissolution (blue line). Both spectra are background corrected and are normalised to the highest peak.

Shirin Baydjanova

Appendix B. SEM images of organic matter of the samples from the Balcanoona Formation and the Rasthof Formation.
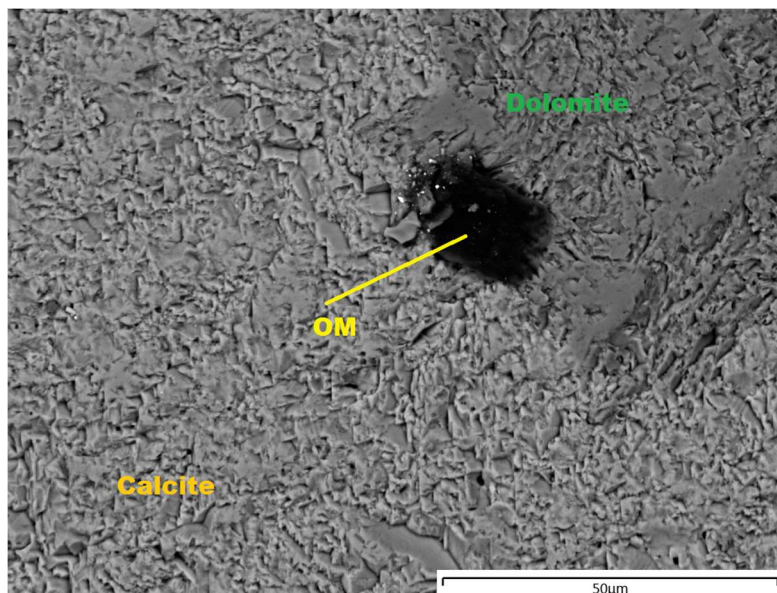
Figure B.1. AK019, site 11 Representative back scattered electron image of OM between dolomite (dark grey) and calcite (light grey) grains in AK019.
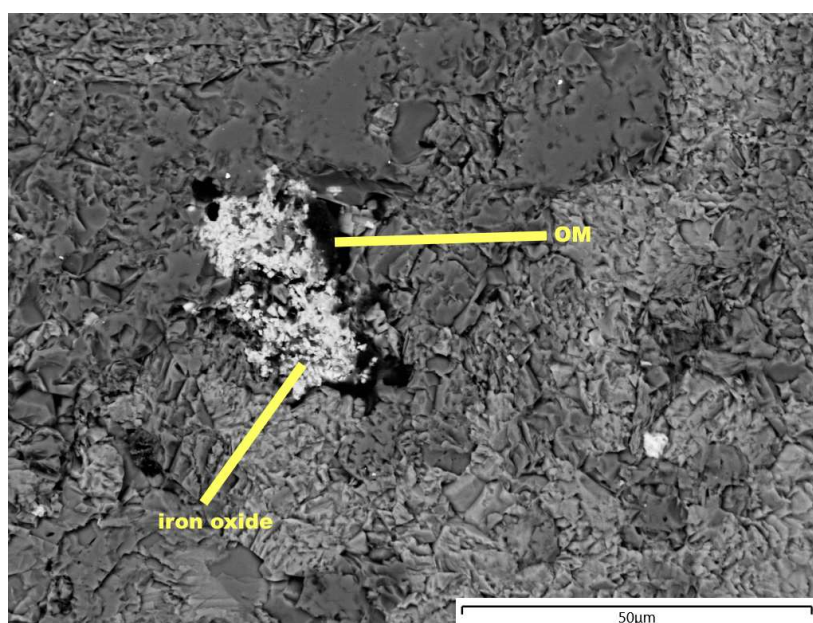
Figure B.2. Representative back scattered electron image of amorphous OM around an iron oxide grain in AK019.

Shirin Baydjanova
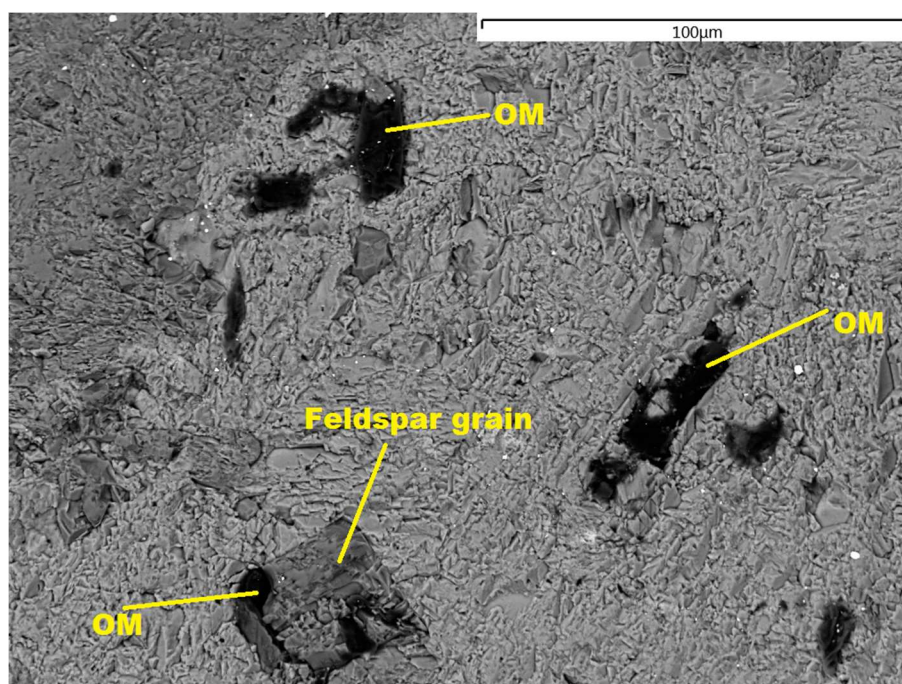
Figure B.3. Representative back scattered electron image of AK019 showing structured OM in a carbonate matrix. Note the amorphous OM spots on a plagioclase feldspar grain. The matrix is calcite (light grey) and dolomite (dark grey).
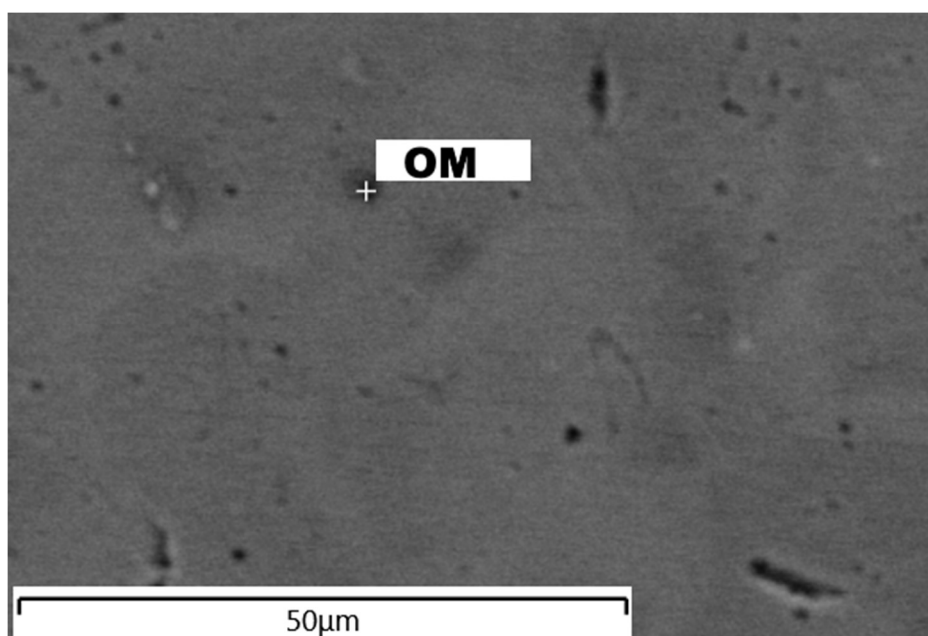
Figure B.4. Back scattered electron image of carbonate matrix and OM (Huab North 2, spot marked with a cross).

Shirin Baydjanova

# Appendix C. Partial chromatograms of N (m/z 128), MN (m/z 142), and xylenes (m/z 106).
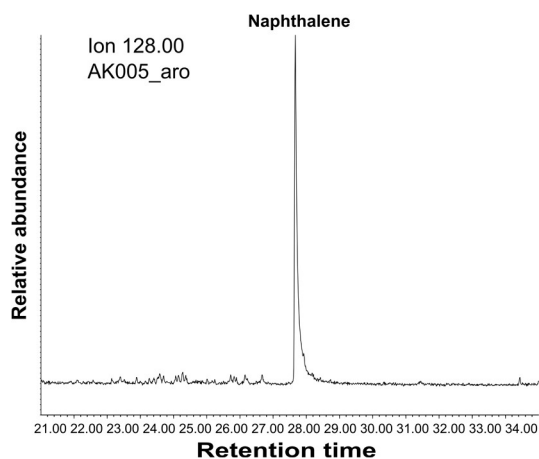
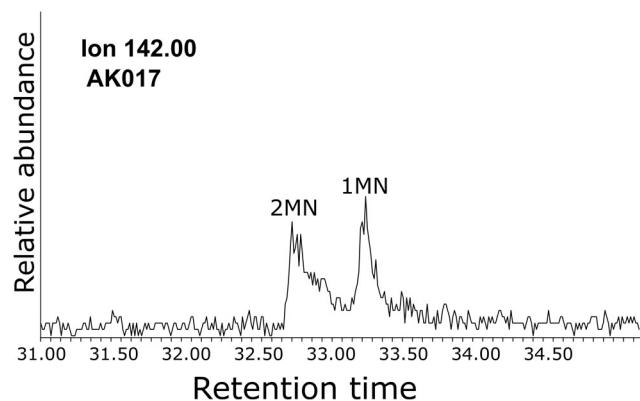Figure C.1. Partial m/z 128 chromatogram of sample AK005 showing naphthalene.
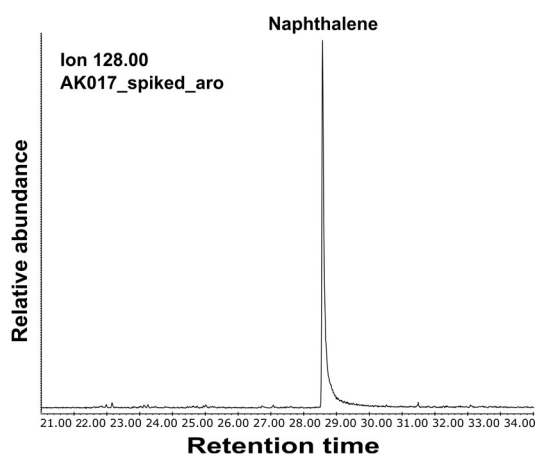
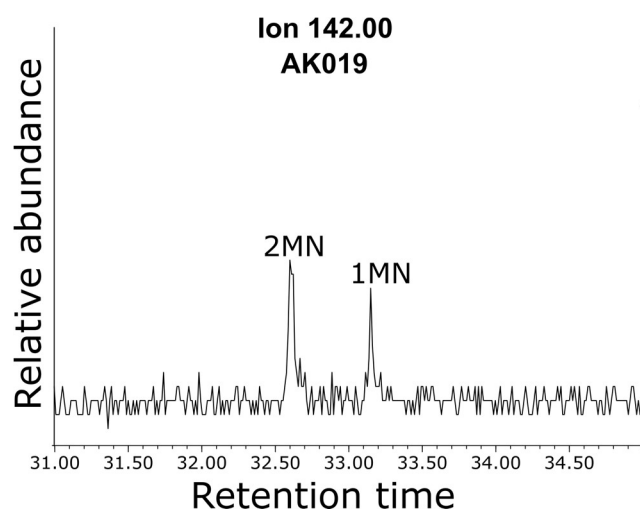

Figure C.2. Partial m/z 128 chromatogram of sample AK017 showing naphthalene.
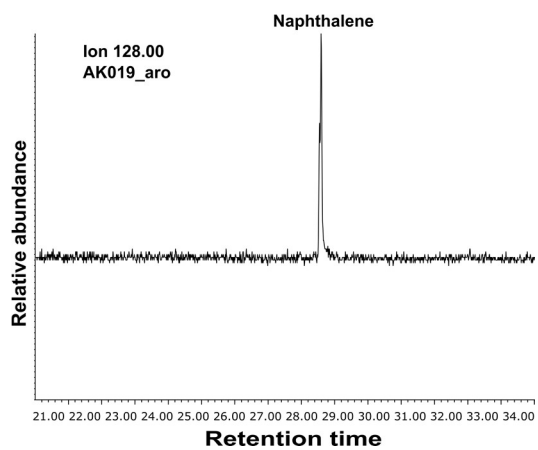
Figure C.3. Partial m/z 128 chromatogram of sample AK019 showing naphthalene.

Shirin Baydjanova
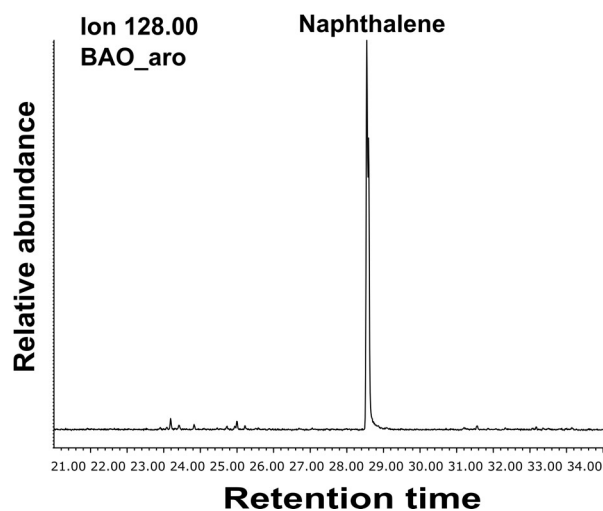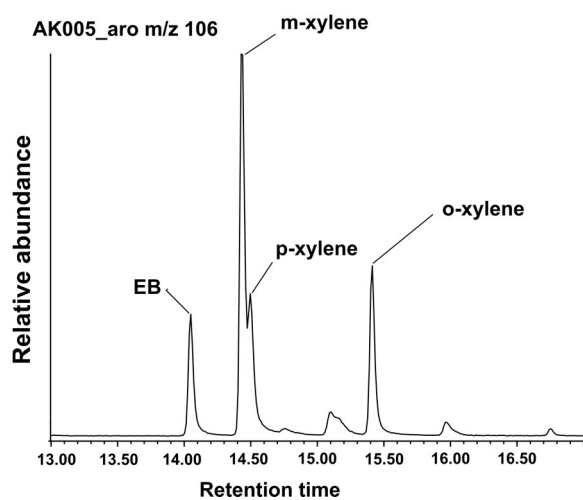
Figure C.4. Partial m/z 128 chromatogram of sample Bao-2A showing naphthalene.
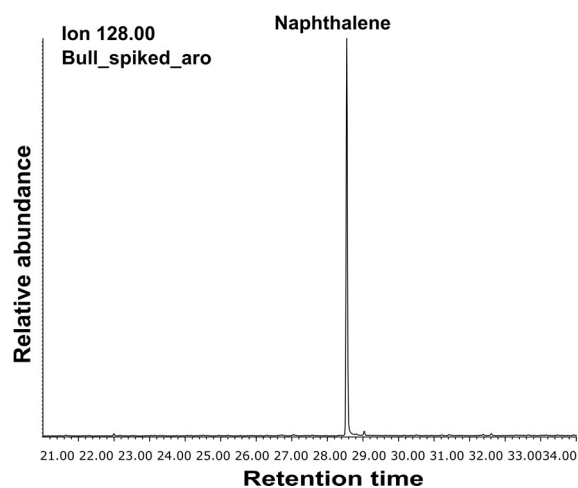
Figure C.5. Partial m/z 128 chromatogram of sample Bull showing naphthalene.
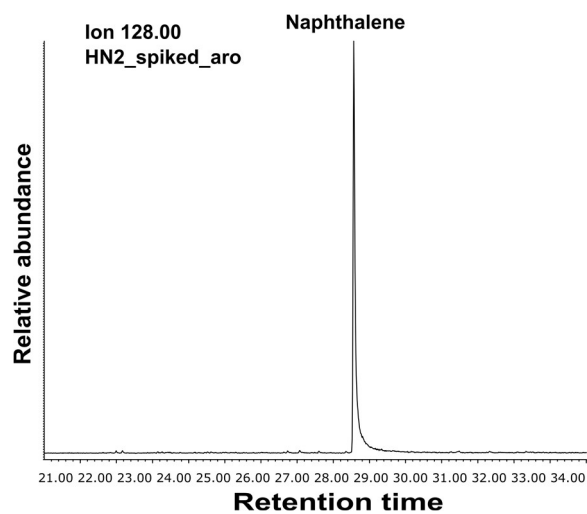
Figure C.6. Partial m/z 128 chromatogram of sample Huab North 2 showing naphthalene.

Shirin Baydjanova
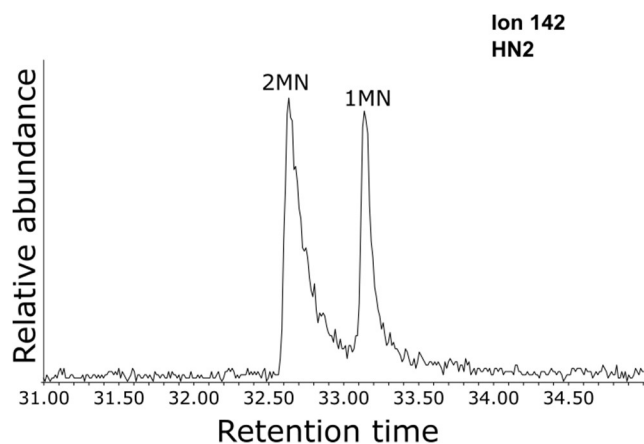
Figure C.7. Partial m/z 142 chromatogram of sample Huab North 2 showing methylnaphthalenes.
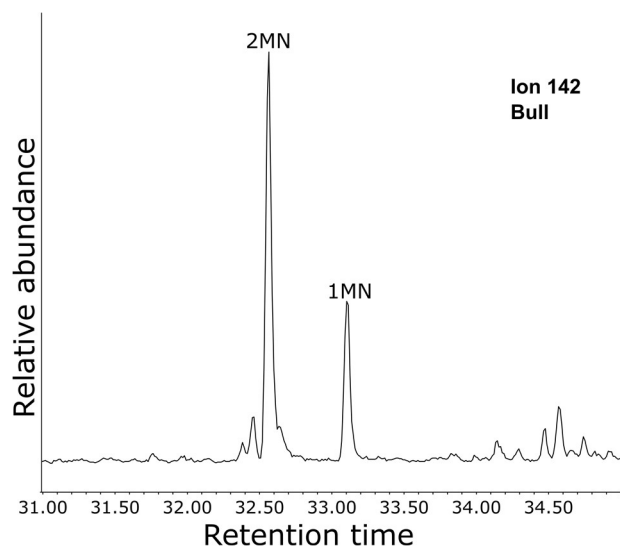
Figure C.8. Partial m/z 142 chromatogram of sample Bull showing methylnaphthalenes.
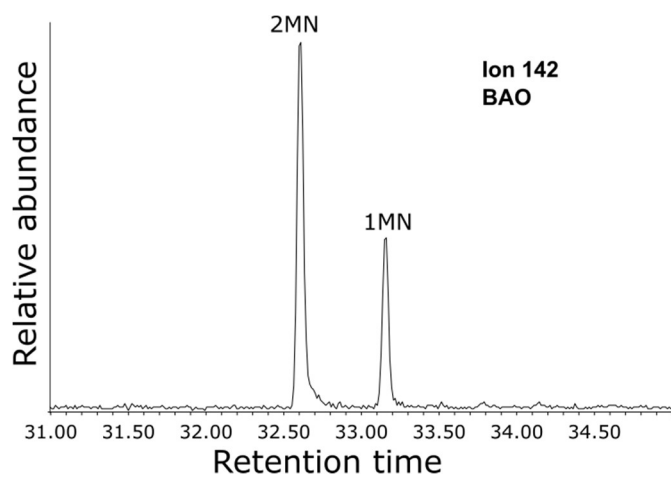
Figure C.9. Partial m/z 142 chromatogram of sample Bao-2A showing methylnaphthalenes.

Shirin Baydjanova
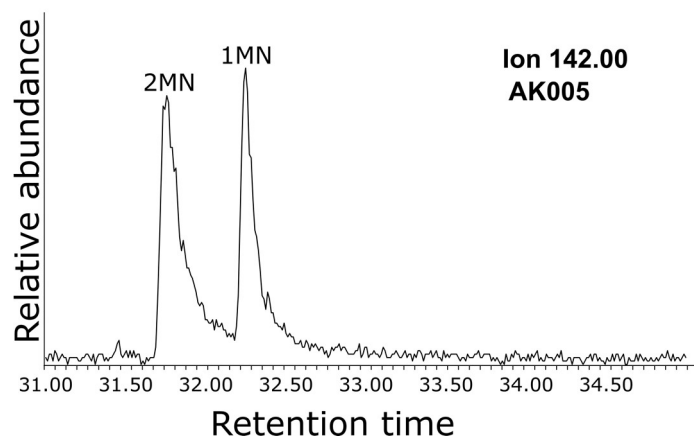
Figure C.10. Partial m/z 142 chromatogram of sample AK005 showing methylnaphthalenes.

Figure C.11. Partial m/z 142 chromatogram of sample AK017 showing methylnaphthalenes.

Figure C.12. Partial m/z 142 chromatogram of sample AK019 showing methylnaphthalenes.
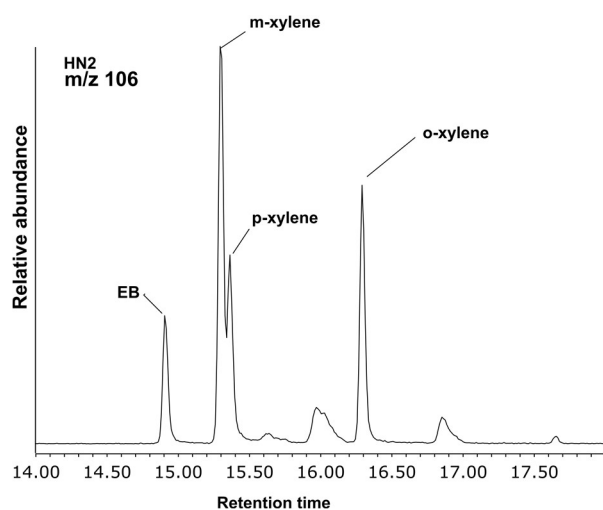
Shirin Baydjanova

Figure C.13. Partial m/z 106 chromatogram of sample AK005 showing xylenes.

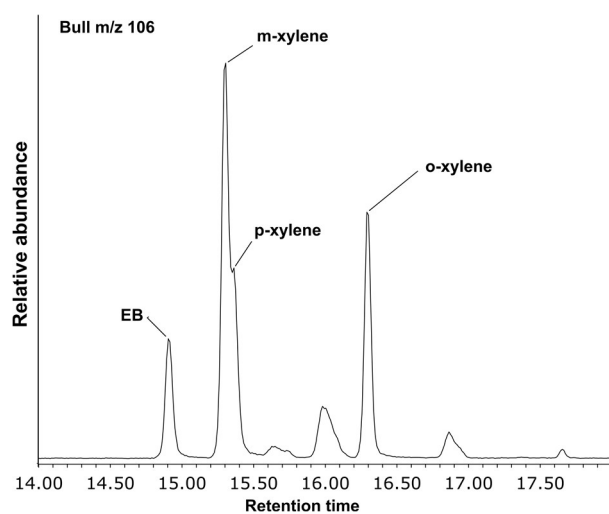Figure C.14. Partial m/z 106 chromatogram of sample HN2 showing xylenes.

Figure C.15. Partial m/z 106 chromatogram of sample BULL showing xylenes.
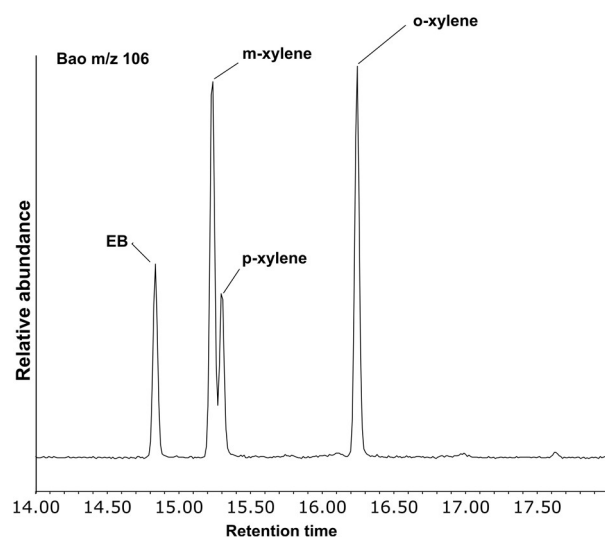
Shirin Baydjanova

Figure C.16. Partial m/z 106 chromatogram of sample Bao showing xylenes.
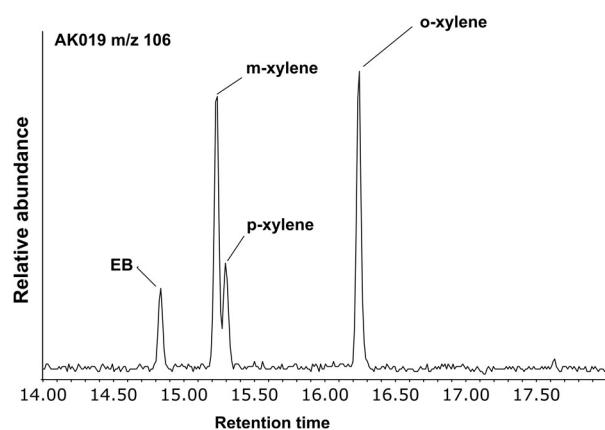

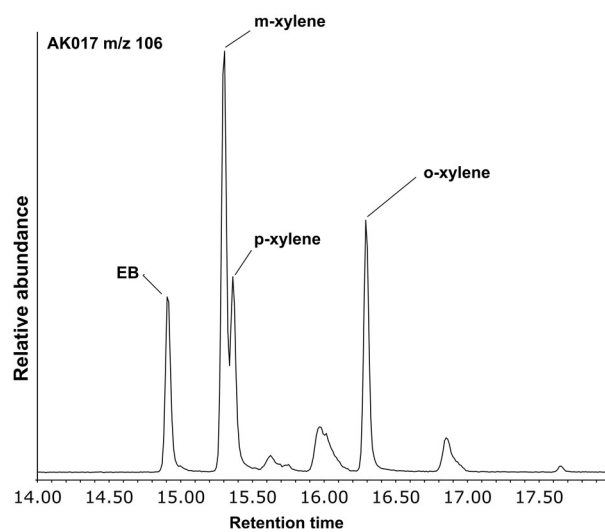Figure C.17. Partial m/z 106 chromatogram of sample AK019 showing xylenes.

Figure C.18. Partial m/z 106 chromatogram of sample AK017 showing xylenes.

Shirin Baydjanova